"TRANSPARENT CONDUCTING SnO_2:F THIN FILMS FOR SIS SOLAR CELLS"

BY

MWABORA JULIUS MWAKONDO

Thesis submitted in partial fulfilment for the degree of Master of Science of the University of Nairobi.

SEPTEMBER 1992

DECLARATION

This thesis is my original work and has not been
presented for a degree in any other University.

mwabora

MWABORA JULIUS MWAKONDO
UNIVERSITY OF NAIROBI

This thesis has been submitted for examination with the
approval of my University supervisors

Dr. A. K. RATURI
Department of Physics
University of Nairobi
P. O. BOX 30197
NAIROBI

Dr. E. SARHENE
Department of physics
University of Nairobi
P. O. BOX 30197
NAIROBI

A C K N O W L E G D E M E N T .

In writing this thesis I have received helpful criticisms throughout and suggestions from many people. In particular I must mention my gratitude in this connection to my supervisors, Dr. A. K. Raturi and Dr. E. Sarhene.

Grateful acknowledgement is made to chemistry department for use of its laboratory and equipment. I would also like to thank technical staff both in the department of Physics and Chemistry for their unfailing support.

I must also thank my colleagues for invaluable and moral support. Grateful acknowledgement and thanks are due to Mr. Mbugua Zakayo, Mr. George Odhiambo and Mr. Phillip Mutonyi for their excellent art work produced from the writers sketches.

Above all, however, I must express my indebtedness to the University of Nairobi for providing a scholarship to enable me undertake this study.

A B S T R A C T

Chemical vapour deposition has been used to deposit transparent conducting tin oxide thin films. The films are useful for solar energy applications. Optical and electrical properties have been investigated. Direct and indirect bandgap values of tin oxide films have been found to be 3.55 and 3.19 eV respectively. Transmission in the visible region of the spectrum was about 85%.

Preparation of Fluorine doped tin oxide films is also presented. The sheet resistance obtained is 50Ω per square. An attempt was made to fabricate $SnO_2:F/SiO_2/p-Si$ solar cell which yielded an open circuit voltage of 0.25 V, short circuit current density of $556\mu A/cm^2$, fill factor of 0.23 and efficiency of 0.04% under $80mW/cm^2$ insolation. The low efficiency can be attributed to high series resistance, mismatch of workfunction and possibly thick interfacial oxide layer.

LIST OF SYMBOLS

R O M A N.

D = Diffusion coefficient

D_n = Electron diffusion coefficient

D_p = Hole diffusion coefficient

E = Electrostatic field

E_C = Semiconductor conduction band

E_{COS} = Oxide semiconductor conduction band

E_F = Semiconductor valence band

E_{FE} = Quasi Fermi level for hole

E_{FOS} = Oxide semiconductor conduction band

E_V = Semiconductor valence band

E_{VOS} = Oxide semiconductor valence band

E_g = Band gap

E_{gi} = Insulator band gap

E_{gos} = Oxide semiconductor band gap

E_{gs} = Semiconductor band gap

FF = Fill Factor

G = Generation rate

h = Plancks constant

I = Current

I_0 = Diode injection current

I_1 = Light generated current

I_D = Dark current

I_L = Photocurrent

I_{mp} = Current corresponding to maximum power point

I_{sc} = Short circuit current

J_D = Dark current density

J_0 = Diode injection current density

J_n = Electron current density

J_p = Hole current density

J_{re} = Current density due to interface recombination

J_{sc} = Short circuit current density

J_{th} = Current density due to interface recombination

J_{ts} = Subsequent emission current density

k = Extinction coefficient

$\vec{k}$ = Crystal momentum

K = Boltzman constant

$\vec{K}$ = Wavevector

L = Diffusion

L_n = Diffusion length for electrons

L_p = Diffusion length for holes

m = Ideality factor

n = Refractive index

n_i = Intrinsic carrier density

P_{in} = Power input

q   = electronic charge

R   = Reflectivity

R_s = Series resistance

R_{sh} = Shunt resistance

R_{st} = Sheet resistance

t   = Film thickness

T   = Transmittance

T_a = Tunneling probability of photogenerated electrons

U   = Net thermal recombination-generation rate

V   = Voltage

V_{mp} = Voltage corresponding to maximum power point

V_{oc} = Open circuit voltage

G R E E K.

α = Absorption coefficient

δ = Oxide thickness

ε = Dielectric constant

ε_1 = Real dielectric constant

ε_2 = Imaginary dielectric constant

η = Efficiency

μ = Mobility

μ_n = Electron mobility

μ_p = Hole mobility

τ = Life time

τ_{no} = Electron life time

τ_{po} = Hole life time

ν = Frequency

Φ_B = Barrier height

$\varkappa_a$ = Average barrier height of insulator semiconductor interface

ψ_{osi} = Oxide semiconductor to insulator barrier height

ψ_{si} = Semiconductor to insulator barrier height

ω = Angular frequency

Ω = Frequency of phonons

C O N T E N T S .

LIST OF ILLUSTRATIONS

CHAPTER ONE

INTRODUCTION

1.1 Introduction.

The need to divert from traditional sources of energy
(fossil fuels and nuclear energy) is inevitable because
they are becoming scarce, expensive (as experienced during
the 1991 Gulf war), and environmentally hazardous as
highlighted by the Alaskan disaster [1] and Chernobyl
disaster in the U.S.S.R [2]. Many alternative ways to
obtain energy are conceivable and they are all ultimately
derived from three natural sources of power: the radiation
of the sun, the energy of the tides, and the heat inside the
earth.

1.1.1 Solar energy.

Growing interest for solar energy has led to a great deal
of research around the world. This can be attributed to the
fact that solar energy is abundant and inexhaustible. A
country cannot be cut off from it. Another reason is that
in solar energy conversion there are no harmful
environmental or societal consequences.

The sun radiates in a continuous process of thermonuclear
fission approximately 8.33×10^{25} KWh of energy of energy
into space everyday of which the earth receives about
4.41×10^{15} KWh of energy [3].

The spectral distribution of the solar radiation as

observed outside the earth's atmosphere is as shown in Fig. 1. On the basis of this distribution , the sun can be considered as a black body radiating at a temperature of $6050^{\circ}K$. Most of the solar spectrum lies in the range 0.25 to 2.5 μm with the maximum at 0.55 μm. The energy comes in the form of quanta (i.e photons). Solar spectrum is modified by the atmosphere if we observe it on the earth's surface. The greater the distance light has to travel , the more the spectrum is modified. This effect is conveniently described by defining an air mass number (AMX). AMO is the energy received per unit area outside the earth's atmosphere. AM1 is the energy received per unit area on the earth's surface when the sun is overhead. AM2 is the solar radiation at ground level when the sun is 30° above horizon during a typical clear sky condition. AMO has a light intensity of about 1.38 KWm^{-2} while AM1 has a light intensity of about 1 KWm^{-2} with a maximum of 1.1 KWm^{-2} on high mountains. The path length for a zenith angle is just secant(θ) times the path length for $\theta = 0$. And hence, AMX denotes the path length x times to AM1 where $x = \sec\theta$. The solar irradiation for AM2 is also shown in Fig.1.

For situation on the earth's surface, the description must be extended to account for the prevailing weather conditions. The absorption and scattering of light in the atmosphere due to the following processes can take place:

(i)   Rayleigh scattering

(ii)   Ozone absorbs all the radiation below 0.29 μm wavelength of light
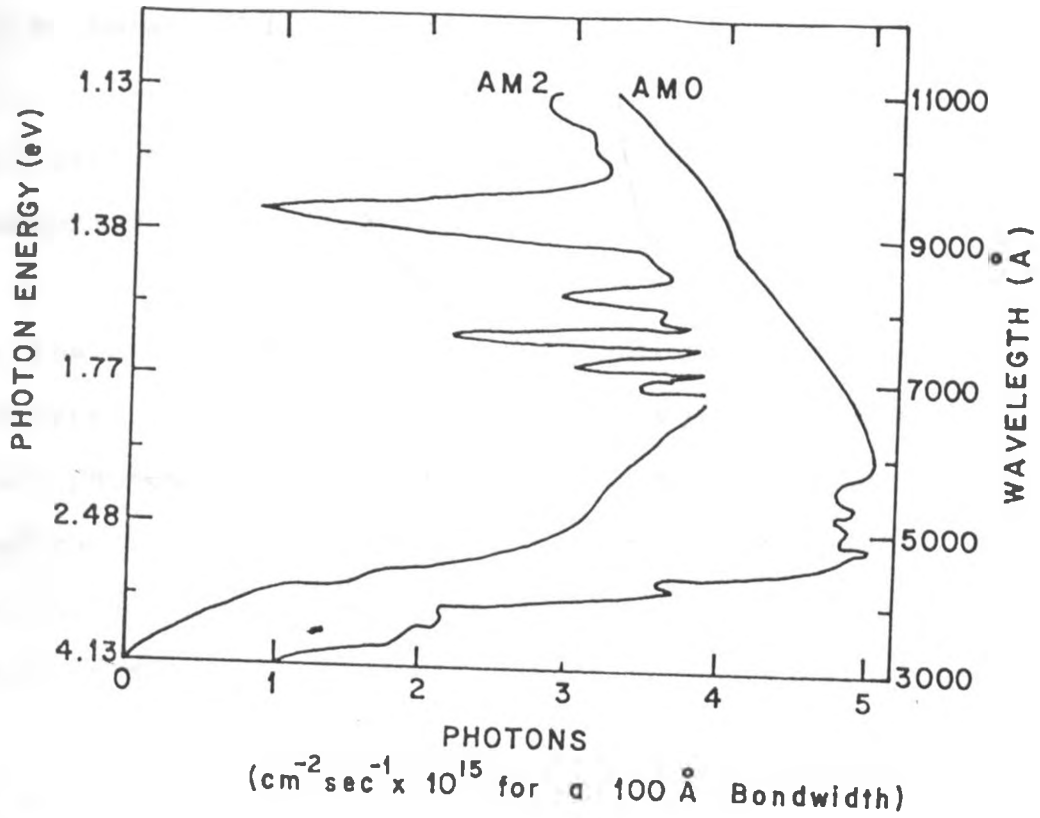
Fig. 1   The spectral distribution of solar radiation
[4]   for   AMO   and   AM2.

(iii) Molecular rotational and vibrational absorption in H_2O and CO_2. This takes place for wavelengths *greater than* 3.0μm.

(iV) Scattering by aerosols and particulate matter, which is greater for shorter wavelengths.

1.1.2 Solar energy conversion.

Utilization of solar energy can be divided into two categories. These are photovoltaic and photothermal.

In the photovoltaic approach sunlight is directly converted to electricity by using the photovoltaic effect. Solar photons incident on a semiconductor surface generate electron – hole pairs. These pairs are separated by an internal electric field across the solar cell junction which produces an electric current in the external circuit.

In the photothermal approach incident sunlight is absorbed by the absorber surface to generate heat. This surface in a solar absorber should have high solar absorptance and low thermal emittance to suppress thermal radiation losses.

In both the photothermal and photovoltaic systems the optical properties of the surface have a significant effect on the system's performance.

1.1.3 Solar cells.

Solar cells have been identified as a possible solution to the energy crisis. Their attributes as regards pollution, portability and suitability for use for remote and rural development has encouraged many researchers to work on them. It is also due to the fact that it can be fabricated in varying sizes making it adaptable for use in many places.

Solar cells can be categorized into p-n junctions, MIS structures, SIS structures etc. Thin film techniques are recognized to be among the most promising ways of producing low cost solar cells [5]. Basic research in new materials, deposition techniques and fast deposition rate should be encouraged for further cell efficiency and decrease in cell cost. There are many techniques of producing thin films. These are chemical vapour deposition (CVD), sputtering, spray pyrolysis, chemical deposition and high vacuum evaporation, etc.

1.1.4 Window coatings.

These are transparent conducting coatings which either transmit, reflect or absorb sunlight radiation at specific wavelength ranges depending on material. The materials which can be used to prepare such films are $In_2O_3:Sn$, $SnO_2:F$, ZnO etc. The general transmission and reflection curves for such materials are shown in Fig. 2. Transmission is high for a particular wavelength range but

5
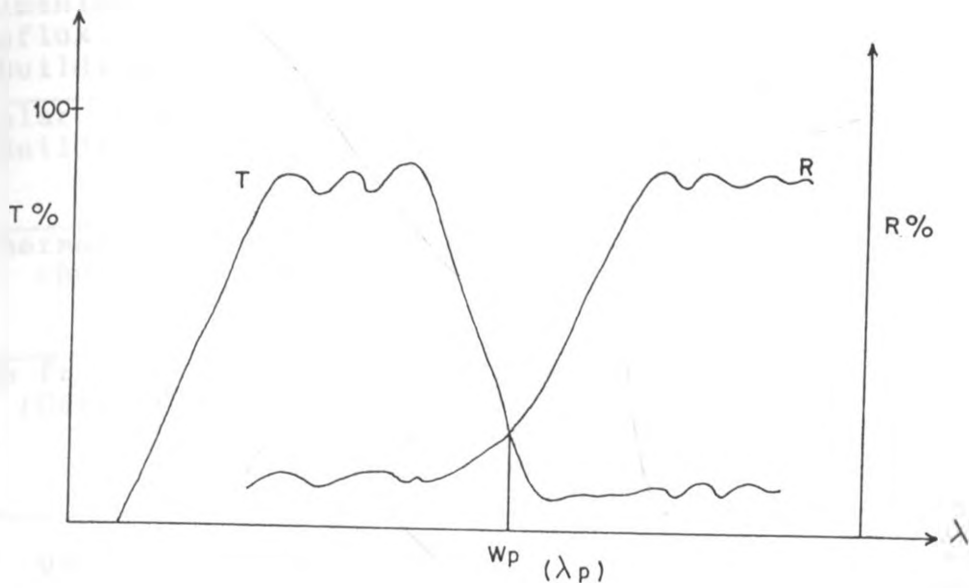
*Fig. 2   The general Transmission and Reflection curves for
window materials.*
[6]

drops suddenly with decreasing wavelength corresponding to
the absorption edge of the film. The film is thus opaque
to this kind of radiation. To the right (in the Near
Infra Red--Infra-Red (NIR--IR) region) the film absorbs
all the radiation due to absorption by free carriers. The
reflection curve follows an opposite pattern (ie. reflection
is low in the visible region and increases in the I-R
region). At plasma frequency the two curves intersect.

Window coatings are of interest because they can be used to
reduce the problems associated with sunlight radiation.
Table 1 shows the problem and the material which can be
used to solve the problem.

Table 1. *Application of window coatings.*

Problem	Solution	Material
Diminish solar influx (Buildings, Cars)	Reflect at o.3-3 μm	TiO_2 / Ag / TiO_2
Solar heating (Building, Cars)	Absorb at 0.7-3 μm and reflect at 3-100 μm on inside	In_2O_3:Sn , SnO_2:F
Thermal insulation (Building)	Reflect at 3-100 μm	In_2O_3:Sn , SnO_2:F
No frost, no mist (Cars, Planes)	Reflect at 8-13 μm on outside, Electrical heating, High conductance	SnO_2:F
UV Protection	Absorption at bandgap	ZnO

1.1.4.1   Application of transparent coatings for solar energy utilization.

(i) Photothermal.

Transparent conducting coatings (SnO_2, In_2O_3, ZnO etc.) transmit the visible region of solar radiation, but have high infrared reflectivity. When suitably doped they can be used as heat mirrors.   The plasma refection edge shifts with carrier concentration and   the   properties   of these coatings can therefore be made to   correspond   to   an ideal heat mirror[see Fig. 3].
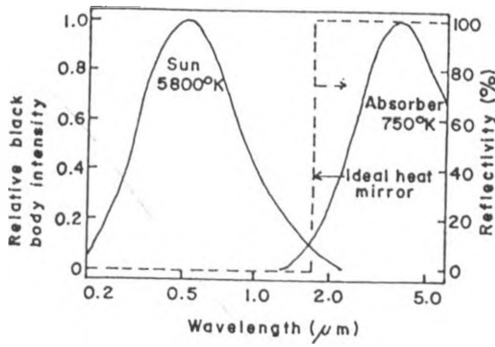
*Fig. 3   Normalized distribution of radiant energy for
[7]   blackbody temperatures of 5800°K (solar
           distribution at AMO) and 750 °K .*

The efficiency of a solar collector system can be increased

by increasing the operating temperature.   This can be done

by reducing   the   Infra-Red (I-R)   emission   from   the

collector by coating SnO_2:F film on the inside of glass   in

the collector [see Fig. 4   ].
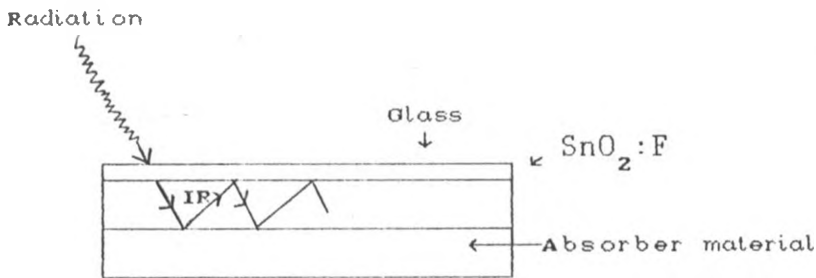
*Fig. 4   Figure to show how I-R emission from   collector
          is reduced by coating SnO_2:F.*

(ii) Photovoltaic SIS   structures.

The most promising structures   used   for   SIS   solar   cells

are SnO_2:F/SiO_2/Si, In_2O_3:Sn/SiO_2/Si   and ITO/SiO_2/Si   [8,9].

8

The properties of window coatings which make them ideal for solar cells are given below:

1. $SnO_2:F$, $In_2O_3:Sn$ have optimum refractive index to provide an inherent antireflection coating on silicon. For antireflection coating, the refractive index (n) of material should be [10]

$$n = \sqrt{n_1 n_2} \qquad \dots\dots\dots\dots\dots (1)$$

where n_1 and n_2 are refractive indices of silicon and air respectively. The refractive indices of air and silicon are 1.000292 and 3.448 respectively [11]. Hence the refractive index of the antireflection coating for Silicon using equation 1 should be 1.86. The refractive index of SnO_2 is 1.9 hence it serves as an ideal antireflecting coating [12].

2. Low resistivity simplifies making front contact.

3. These materials ($SnO_2:F$, $In_2O_3:Sn$) absorb in the ultraviolet and transmit visible radiation, therefore act as window materials.

4. They serve as active components of the solar cells.

5. The thin films of the window materials can be fabricated by cheaper and simpler methods.

1.2 Literature review.

Solar cells have been known for quite some time. Their advancement have been rather slow due to technological

9

limitations.

Suggestions for the development of the solar cells was given by Lange in 1930 [13]. Later in 1954 Pearson, Fuller and Chapin made first practical solar cell [14]. The photocell was made to deliver power from the sun into a resistance load at the rate of 60 Watts per square meter of photocell surface giving an efficiency of 6%. Since then development has been going on in different parts of the world, the main aim mostly being to improve the efficiency and minimizing fabrication costs.

Solar cells made from single crystals are not economical [15]. The cells should be made as thin as possible in order to reduce cost of material. The ideal materials with thickness of about $1\mu m$ can easily be obtained by thin film deposition methods such as evaporation, sputtering, or chemical vapour deposition. Cost, performance and reliability determine the direction and scope of the worldwide research efforts in developing solar cells. The performance of various polycrystalline thin film solar cells from 1985 to 1989 gives efficiencies ranging between 4.9-12.5% [16].

Transparent conducting coatings of wide band gap semiconductors viz. SnO_2, In_2O_3, Cd_2SnO_4, are being extensively studied for their applications in solar energy utilization, both photothermal and photovoltaic [17]. These materials have high transmission in the visible range and high Intra-Red (I-R) reflectivity which make

them suitable for applications in solar absorbers. These coatings applied to the inner side of the glass cover are not subjected to the same humidity and temperature variations as the selective absorber coatings on the absorber surface [7]. These films are also used to control the internal environment of buildings by their application to windows.

Transparent conducting coatings have also been used as the top layer in SIS photovoltaic systems [18] where they act as antireflecting layer because of their high refractive index, as a transparent conducting electrode and as an active element of the solar cell. Singh et al [8] fabricated SIS solar cells comprising chemically deposited SnO_2:F and In_2O_3:Sn, a thin SiO_x layer grown in concentrated HNO_3 and n-Si substrates with (100) yielding an efficiency of about 11%. ITO based SIS solar cells were fabricated by Feng et al [9] and Chang and Sites [19] yielding conversion efficiencies of 9.85% and 12% respectively.

Tin oxide films have been extensively studied since their high transmission in the visible range, high I-R reflection and high conductivity makes them suitable for solar energy applications. Tin oxide film is an n-type semiconductor material with a direct band gap of 4 eV and indirect band gap of 2.6 eV [20]. These band gap values allow SnO_2 films to be transparent in the entire visible region of the spectrum. The electrical and optical properties of doped SnO_2 films have been investigated by various authors

[21,22]. The absorption edge of thin SnO_2 films is around 3.7 eV, the position depending upon free electron concentration. These films have been prepared by various methods viz spray pyrolysis [22], vacuum evaporation [23], chemical vapor deposition [24] etc. Recently Vlahovic and Persin have developed a simple CVD technique for growing SnO_2 films [25].

Some work on solar cell fabrication has been carried out in Physics laboratory, University of Nairobi. Manyonge [26] in 1981 developed ceramic CdS/CuS solar cells. He calculated the efficiency of the solar cell and found it to be approximately 0.0012%. Ogola [27] in 1985 fabricated silicon solar cell by introducing elemental phosphorus into silicon through a layer of molten phosporosilicate glass. The efficiency of that cell was found to be 1%. Finally Kalaiya [13] fabricated Semiconductor Insulator Semiconductor (SIS) photovoltaic converters by spray pyrolysis and vacuum deposition techniques. The efficiencies of the two photovoltaic converters were 0.002% and 0.85% respectively under $80mW/cm^2$ insolation.

1.3 Objectives of the present work.

The main objective of this study was to prepare highly transparent and conducting SnO_2:F thin films by a simple CVD technique for solar energy applications. The deposition parameters were to be established and SIS solar cells incorporating these films were to be fabricated.

THEORETICAL   BACKGROUND

2.1   Tin oxide structure.

Tin oxide exists in three different modifications of which the rutile form (in the mineral cassiterite) is the most common [28].   It   is   insoluble   in   water   and scarcely attacked at all by acids or alkalis   except   when they are   concentrated   and   hot,   it   dissolves   in   fused alkalis to give   stannates   or   the   presence   of   sulphur thiostannates [29].

The structure for tin oxide is ionic.   In an ionic structure each ion is surrounded by   a   certain   number   of   ions   of opposite signs, this   number   is   called   the   coordination number.   The unit cell of the crystal structure of SnO_2 is shown in Fig. 5.
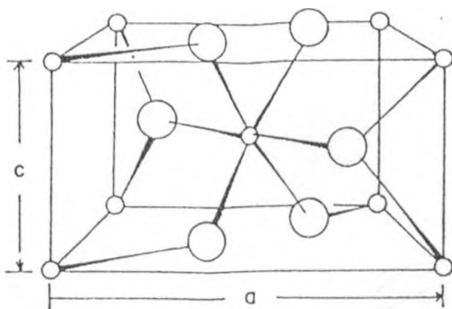
Fig.   5.   Unit cell of the crystal structure of SnO_2.
  [7]   *The large circles indicate oxygen   atoms   and*
            the small circle indicate tin atoms.

The lattice parameters of SnO_2 are a = b = 0.4737 nm and c = 0.3185 nm. The c/a ratio = 0.673. The ionic radii of O^{2-} and Sn^{4+} are 0.14 and 0.071 nm respectively. It is n-type wide band gap semiconductor. It is conducting because of the native defects in pure crystals due to oxygen vacancies.

2.2 Optical properties.

2.2.1 Direct and indirect transitions

Depending on the band gap, semiconductor crystals are either those with direct gap and those with indirect gap. The band gap is the difference in energy between the lowest point of the conduction band and the highest point of the valence band. The lowest point in the conduction band is called the conduction band edge; the highest point in the valence band is called the valence band edge.
Figs. 6 (a) and (b) show direct and indirect optical transitions.
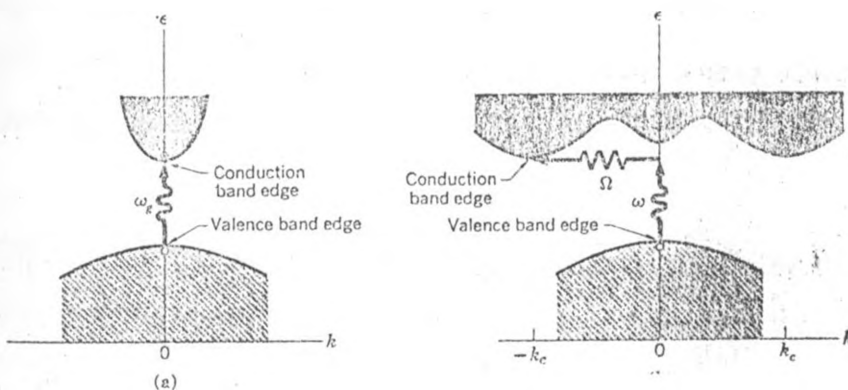
Fig. 6   (a)   Direct optical transition
[30]   (b)   Indirect optical transition

14

In direct transition the lowest point of the conduction band occurs at the same value of $\vec{k}$ (crystal momentum) as the highest point of the valence band . A direct optical transition takes place with no significant change in $\vec{k}$, because the absorbed photon has a very small wavevector. The threshold frequency ω_g for absorption by direct transition determines the energy gap $E_g = \hbar\omega_g$.

The indirect transition involves a photon and a phonon because the band edges of the conduction and valence bands are widely separated in k-space. The threshold energy for the indirect process is greater than the true band gap. The absorption threshold for the indirect transition between the band edges is at $\hbar\omega = E_g + \hbar\Omega$, where Ω is the frequency of the emitted phonon wavevector $\vec{K} = -\vec{k}_c$. At higher temperatures phonons are already present. if a phonon is absorbed along with a photon, the threshold energy is $\hbar\omega = E_g - \hbar\Omega$.

It is important to note that the figure shows only the threshold transitions. Transitions occur generally between almost all points of the two bands for which the wavevector and energy can be conserved.

If the transition probability for the band to band transition becomes constant near the absorption edge [4], then

$$\alpha = \alpha_o (h\nu - E_g)^x \qquad \text{for} \quad h\nu \geq E_g \quad \ldots\ldots\ldots (2)$$

and $\alpha = 0$ for $h\nu < E_g$ . . . . (3)

where $h\nu$ is the photon energy and E_g is the band gap. The following relations hold for different transition.

- $x \approx 1/2$ in relation (2) for direct allowed transition.
- $x \approx 3/2$ in relation (2) for direct forbidden transition.
- $x \approx 2$ in relation (2) for indirect allowed transitions.
- $x \approx 3$ in relation (2) for indirect forbidden transition.

2.2.2 Transmission and reflection.

Optical properties of a medium are characterized by complex parameters. The real part generally gives an idea about dispersion, while the imaginary part provides a measure of dissipation rate of the wave in the medium. Two complex parameters which can be considered are:

(i) the index of refraction given by

$$N = n - ik \quad .... \quad (4)$$

where n is the ordinary index and k is the extinction coefficient

and

(ii) dielectric constant

16

$$\varepsilon = \varepsilon_1 - i\varepsilon_2 \quad \dots\dots\dots\dots\dots\dots\dots\dots\dots \quad (5)$$

where ε_1 and ε_2 are the real and imaginary dielectric constants.

Using Maxwell's equations the two parameters can be joined to give

$$\varepsilon_1 = n^2 - k^2 \ , \quad \varepsilon_2 = 2nk \quad \dots\dots\dots\dots\dots \quad (6)$$

The reflectivity (R) at an absorbing medium of indices (n, k) in air for normal incidence is given by

$$R = \frac{(n - 1)^2 + k^2}{(n + 1)^2 + k^2} \quad \dots\dots\dots\dots\dots\dots\dots \quad (7)$$

and the transmittance equation is given by

$$T = A (1 - R)(1 - R') e^{-\alpha t} \quad \dots\dots\dots\dots \quad (8)$$

when the interference and multiple reflections are neglected. R and R' are reflection coefficients at air-film and film substrate interfaces respectively and A is a constant. Parameters α and t are the absorption coefficient and thickness of the film respectively. The absorption coefficient is related to the extinction coefficient by the expression $k = \frac{\alpha\lambda}{4\pi}$, where λ is the wavelength.

2.3 Solar cells.

2.3.1 Introduction.

For any development in solar cell technology it is necessary to understand the photovoltaic effect as solar cells operate on this principle. Photovoltaic effect occurs in semiconductors as well as other materials.

2.3.2 The photovoltaic effect.

This is the generation of electrical energy as a consequence of the absorption of ionizing radiation. For solar cell purposes the radiation of interest is photons of light.` Photons absorbed in a semiconductor release their energies to electrons in the valence band, causing them to rise to the conduction band. Thus electron-hole pairs (EHP's) are created, giving an excess above the equilibrium concentration. The rate of generation of EHP's at distance x into the semiconductor is given by

$$G(\lambda, x) = \alpha(\lambda) N_o(\lambda) \exp[-\alpha(\lambda) x] \quad \ldots\ldots\ldots \quad (9)$$

where $\alpha(\lambda)$ is the absorption coefficient for the wavelength λ and $N_o(\lambda)$ is the number of incident photons per unit area per second at that wavelength at the surface.

The absorptivity $\alpha(\lambda)$ is a quantitative measure of the ability of a material to absorb light of a given wavelength and is measured in units of reciprocal distance. In an

18

indirect band gap material [e.g. silicon where the maximum of the valence band and the minimum of the conduction band occurs at different values of crystal momentum, $\vec{k}$], there must be interaction of a photon, an electron, and a phonon from the crystal lattice to satisfy the momentum conditions before absorption of a photon can take place.

Once excess EHP's are generated they must be separated, moved to an edge of the semiconductor and removed to an external circuit before any useful power may be obtained from the incident photons. To effect the separation an electrostatic field must be supplied.
This can be done by creating a p-n junction.

2.3.3 p-n junction solar cell.

The starting material can be an appropriately boron-doped (p-type) single crystal. Phosphorous is diffused into the substrate to create a shallow (0.2-0.5 μm) n-type layer. The layer (front surface) is contacted by a metal grid designed to cover only a small percentage of the surface, while the p-layer is contacted at the back by a metal covering the complete surface. An antireflection coating is used on the front to minimize reflections from the silicon surface between the grid fingers and a cover glass is employed to protect the device in it's working environment. Fig. 7 indicates the form of the energy band diagram in one dimension through the non-metalized region of the cell.

n-region

Light

p-region

E_c
E_i
E_f
E_v
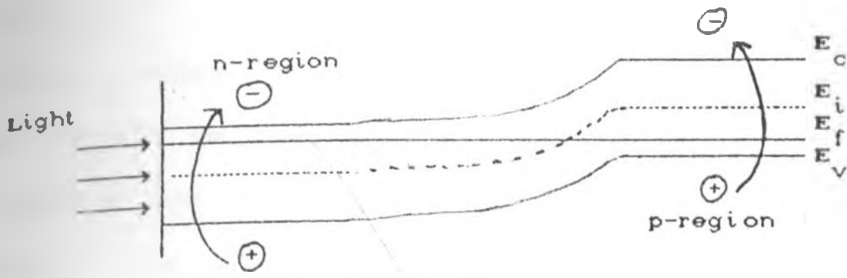
Fig. 7   Energy band diagram in one dimension through the
non-metalized region of the cell.

Short wavelength light will generate excess EHP's near the
front s face where holes are in minority.   Longer
wavelengths will generate excess EHP's in the p-type
substrate where electrons are in minority.   If   in   their
random wanderings excess minority carriers   encounter   the
junction depletion layer they will be   swept   across   the
junction by the electric field.   If no external connections
are made, a voltage will   build   up   across   the   depletion
region as the charge separation occurs,   forward   biasing
the n-p junction. At   steady   state   the   voltage   produced
diode injection current will be equal to photocurrent,   and
the open-circuit voltage (V_{oc}) condition will established.

Equivalent circuit of the cell is shown in Fig. 8

$I_D(V)$

I_L

V
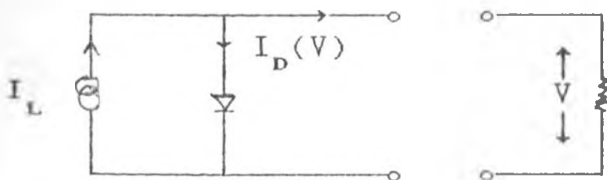
Fig. 8   Model for ideal solar cell

When an external load is connected across the solar cell, current will flow and useful power will be delivered. The voltage across the diode will be reduced from the open-circuit value, hence the diode injection current will be reduced and the external current will be the difference between the photocurrent I_L and the diode current (dark current), $I_D(v)$. Thus

$$I_o(v) = I_L - I_D(v) \quad \dots\dots\dots\dots\dots\dots\dots\dots \quad (10)$$

The basic semiconductor device equations in one dimension (eg. from front to back of the cell) are [31] :

(a) Current transport equations

$$J_n = q\mu_n nE + qD_n \frac{dn}{dx} \quad \dots\dots\dots\dots\dots\dots\dots \quad (11)$$

$$J_p = q\mu_p pE + qD_p \frac{dp}{dx} \quad \dots\dots\dots\dots\dots\dots\dots \quad (12)$$

(b) Continuity equations

$$\frac{\partial n}{\partial t} = G - U + \frac{1}{q}\frac{dJ_n}{dx} \quad \dots\dots\dots\dots\dots\dots\dots \quad (13)$$

$$\frac{\partial p}{\partial t} = G - U - \frac{1}{q}\frac{dJ_p}{dx} \quad \dots\dots\dots\dots\dots\dots\dots \quad (14)$$

(c) Poisson's equation

$$\frac{\partial E}{\partial x} = \frac{q}{\varepsilon} (N(x) + p - n) \quad \dots\dots\dots\dots\dots\dots \quad (15)$$

where J_n and J_p are electron and hole current densities respectively, E is the electrostatic field, μ is the mobility, D is the diffusion coefficient, q is electronic

charge, $N(x)$ is the impurity density distribution. G, the generation rate due to light, is the integral over all wavelengths λ of the right hand side of equation (9). The term U is the net thermal recombination-generation rate, modeled by Shockly-Read-Hall in terms of a trapping level located in the bandgap and is given by

$$U = \frac{pn - ni^2}{\tau_{po}(n+n_1) + \tau_{no}(p+p_1)} \quad \ldots\ldots\ldots\ldots\ldots\ldots \quad (16)$$

Here ni is the intrinsic carrier density, τ_{po} and τ_{no} are minority hole and electron lifetimes respectively and n_1 and p_1 are the electron and hole densities which exist if the Fermi level were located at the trapping level.

The solutions of the above equations give valuable information pointing the way to optimum solar cell design. For purposes of visualizing which parameters are significant, it is useful to introduce approximations and derive analytical solutions. Considering diffusion only and ignoring G, the dark current density of the diode is given by the familiar diode equation [32]

$$J_D(V) = J_o[\exp(qV_j / KT) - 1] \quad \ldots\ldots\ldots\ldots\ldots \quad (17)$$

where I_D and I_o in equation 10 are simply J_D and J_o multiplied by the total area of the junction. For a non ideal case the dark current can be represented by

$$I_D(V) = I_o[\exp(qV / mKT) - 1] \quad \ldots\ldots\ldots\ldots\ldots \quad (18)$$

where m is the ideality factor with values between 1(ideal) and 2.

2.4 Semiconductor Insulator Semiconductor (SIS) solar cells.

2.4.1 Introduction.

Solar cells are mostly formed by creating a p-n junction as illustrated in Fig. 9a. The top layer is generally heavily doped to degeneracy.
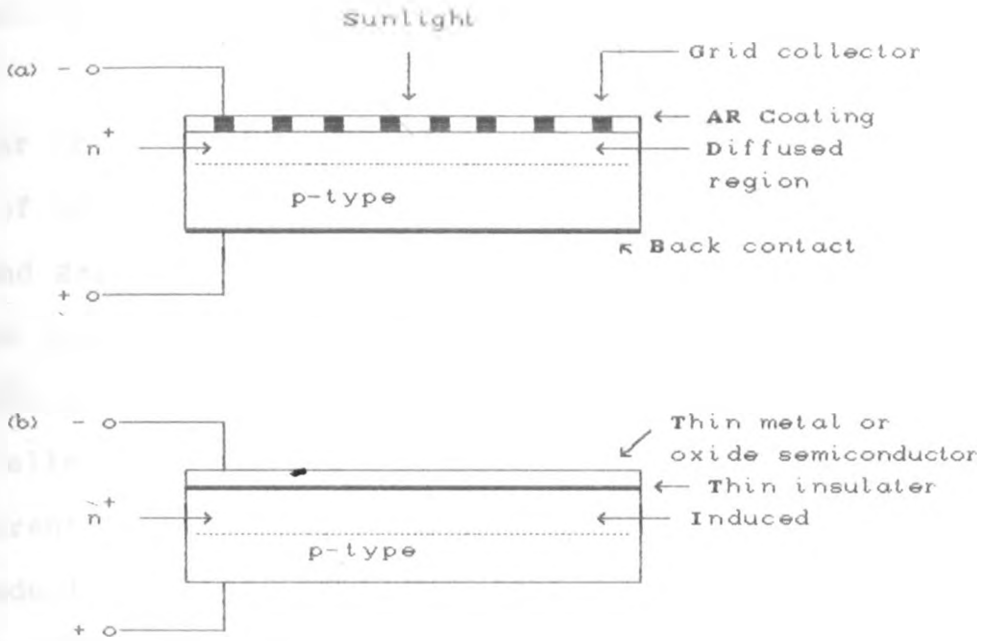
Fig. 9 (a) Conventional p-n junction solar cell with
[33]   diffused n^+ region into p-base semiconductor.
        (b) MIS or SIS solar cell with thin intefacial layer.

The diffusion process to create a p-n junction is a costly one. Extensive search for alternative and potentially lower cost methods of forming a photovoltaic barrier or junction has been going on. One of these techniques consists of inducing a conductivity type change at the surface of the semiconductor by application of ultra-thin metal or

23

relatively thick transparent (wide band gap) conducting semiconductor. This configuration is illustrated in Fig. 9b. Such cells rely on a thin interfacial layer (1-3 nm) between the top "inducing" contact (metal or conducting semiconductor) and the base semiconductor. The interface layer is generally an oxide or some other compound which is normally an insulator in its bulk form. Hence these cells are referred to as Metal-Insulator-Semiconductor (MIS) or Semiconductor-Insulator-Semiconductor (SIS) solar cells.

SIS solar cells can be considered as belonging to a family of heterojunctions in which one side is a wide-band gap semiconductor as SnO_2, mated to a much narrower band-gap material such as Si [18]. Their operation was found to be similar to tunnel MIS solar cells [18], except that the metal is replaced by a transparent (wide band gap) conducting semiconductor. These semiconductors are generally oxides such as SnO_2, In_2O_3 or mixtures of both. In effect the oxides serve as transparent conducting metals. However, there is a big difference between the MIS and SIS configuration which ultimately may decide which of these two structures is superior. The MIS diode requires a thin (~ 5 nm) metal film in order to permit sufficient transmission of light, whereas several hundred nm of conducting oxide can be used because it is largely transparent medium. To be fair, the conducting semiconductor must be degenerately doped so that it resembles a metal.

24

The main advantage of SIS solar cells is that, this method of forming photovoltaic junctions is simple and thus potentially very inexpensive. All that is required is a thin 1-3nm insulating layer to serve as interface. A transparent conducting semiconductor is then applied on top by methods which are easy and low cost. In addition to this feature of easy barrier or diode formation, we have a top layer of diode which is induced and therefore, not defected as in the case when it is formed by diffusion. The SIS structure offers further advantages. The fact that the transparent conducting semiconductor permits the transmission of light and at the same time effectively a metal, means that the requirement of collection grid can be greatly reduced or eliminated. Furthermore, the refractive index of these materials is such that they can be used as partial antireflection (AR) coating.

2.4.2 Theory of SIS solar cells.

To understand the operation of MIS and SIS solar cells, there are basic questions that must be studied. These are :

(1) the role of interfacial layer and

(2) which metal or conducting semiconductor should be placed on top of any given base semiconductor, so as to invert the conductivity type of surface immediately underneath the interfacial layer.

It should be clearly understood that the conversion of incoming photons from the sun's radiation to charge carriers occurs in the bulk of the base semiconductor. The top metal or conducting semiconductor and the interface serve merely to define a potential barrier for the photovoltaic collection process.

The suitability is determined by the work function or electron affinity of the material. The general rule for forming an SIS diode is that for an n-type oxide semiconductor, it's electron affinity should be equal to that of the p-type base semiconductor, or in case of an n-type base semiconductor, the electron affinity should be equal to the sum of the bandgap and the electron affinity of the n-type semiconductor [34]. Table 2 shows the different combinations possible [33] The first question will be answered at a later stage, section [2.3.8].

Table 2 Table to show possible oxide semiconductor with
base semiconductor
[33]
(a) p-type base semiconductor

(b) n-type base semiconductor

(a)

Base semi-conductor	Bandgap of the base semi-conductor at $T=300°K$ (eV)	Desired electron affinity of oxide semi-conductor for p-type base semi-conductor (eV)	Possible oxide semi-conductors	Possible AM1 efficiency (%)
Si	1.12	4.05	ZnO, ITO	21
Ge	0.80	4.0	ZnO, ITO	11
InP	1.34	4.4	ZnO, ITO, In_2O_3, $Cd\,SnO_4$	24
GaAs	1.43	4.07	ZnO, ITO	25
CdTe	1.44	4.30	ZnO, ITO Cd_2SnO_4	25
$CuInSe_2$	1.02	4.58	ZnO, ITO, Cd_2SnO_4, Bi_2O_3	18

(b)

Base semi-conductor	Bandgap of the base semi-conductor at $T=300°K$ (eV)	Desired electron affinity of oxide semi-conductor for n-type base semi-conductor (eV)	Possible oxide semi-conductors	Possible AM1 efficiency
Si	1.12	5.17	SnO_2	21
Ge	0.80	4.80	SnO_2	11
InP	1.34	5.74	SnO_2	24
GaAs	1.43	5.50	SnO_2	25
CdTe	1.44	5.74	SnO_2	25
CuInSe	1.02	5.60	SnO_2	18

The energy band diagram for an isotype SIS (like ITO/n-Si) under zero bias, as deduced by I-V measurements, is shown in Fig 10 [4]. Fig 11 shows the energy band diagram under forward bias. Under illumination, the dark current flows opposite to the photocurrent and various ways of carriers flow, shown in this figure, are loss mechanisms for the photocurrent. A photogenerated carrier may combine and subsequently be annihilated in the absorber itself through path 1; it may recombine at the ohmic contact through path 2; carriers which are not able to tunnel the insulator layer may recombine at the interface through path 3. In addition, the photogenerated carriers can flow opposite to the electrostatic field at the interface by thermionic emission through path 4; multistep tunneling through path 5 and by diffusion etc. Two types of mechanisms can be present at the same time. Whatever mechanism is prominent would dominate and would decide the performance of the device. In a system where the back contact is a selective ohmic contact and the base is a life time semiconductor, path 1 and 2 for the loss of photogenerated carriers will be negligible and the dark current is dominated by the current transport mechanism taking place at the junction. The total dark current density is given by

$$J_d = J_{th} + J_{re} + J_{mt} + J_{ts} + J_t \quad \ldots\ldots\ldots\ldots\ldots\ldots (19)$$

where J_t is the current density except thermionic emission,
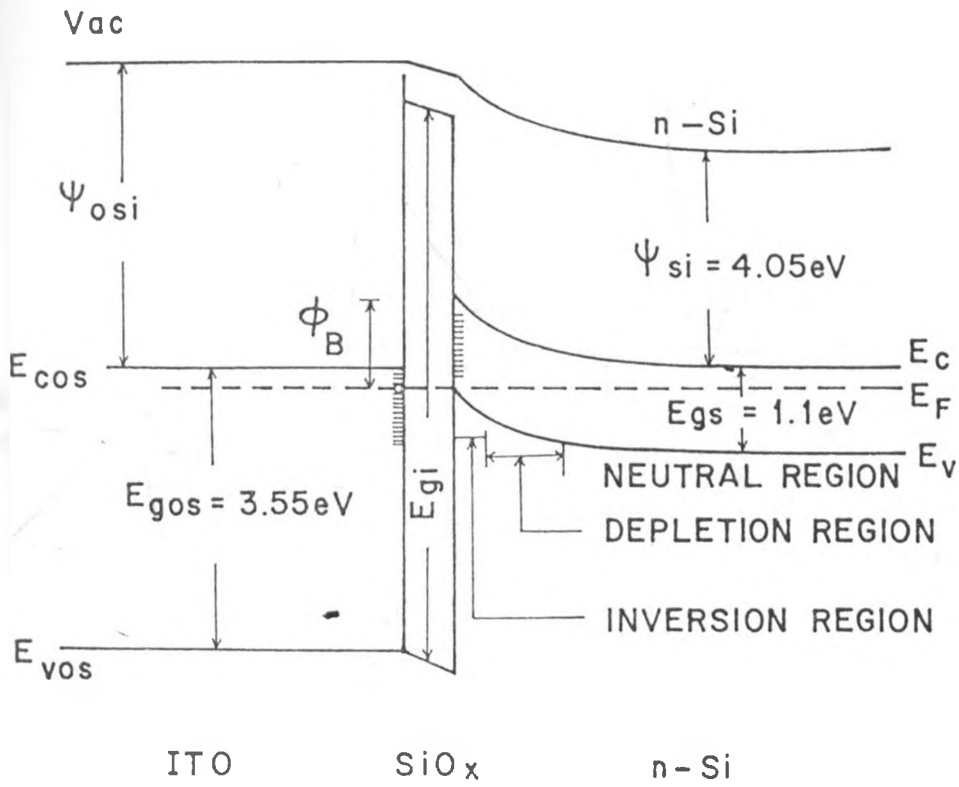
Fig. 10 Energy band diagram for SIS structure
[4]
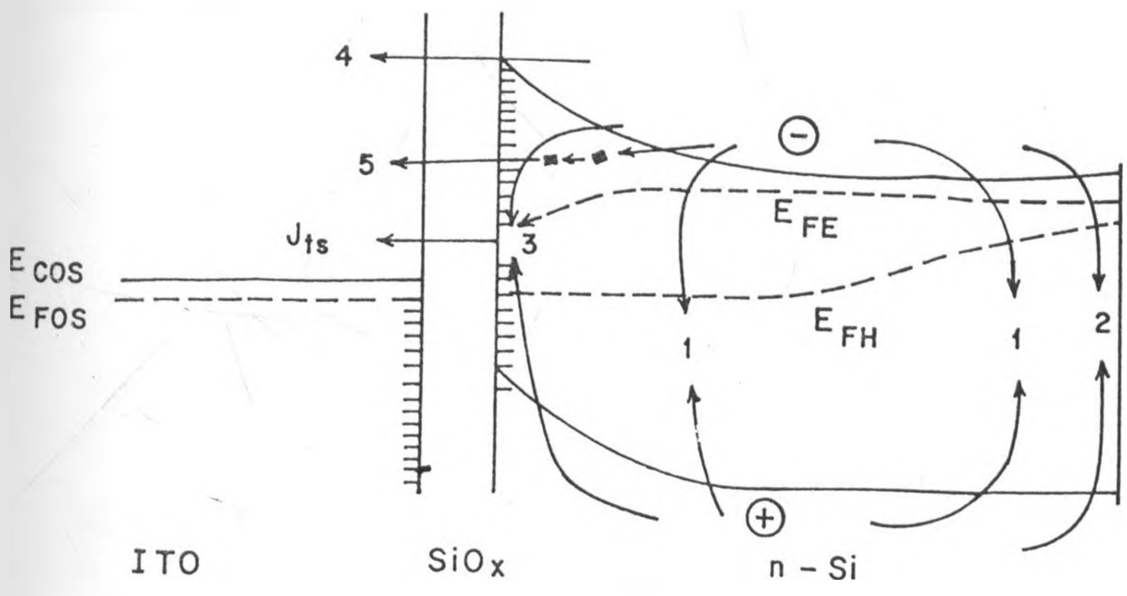
Fig. *11* *Energy band diagram under forward bias*
[4]

interface recombination, multistep tunneling and trapping and subsequent emission current densities. The total current density through the device under light is given by

$$J = J_{sc} - J_d \dots\dots\dots\dots\dots\dots\dots\dots\dots\dots (20)$$

2.4.3 Effect of insulator layer.

The presence of the insulator layer can be advantageous if one or more of the following occurs:

(a) The insulator layer in isotype cell contains the positive charge or decrease the negative charge contained in the localized states at the semiconductor surface. This increases the barrier height and reduces the dark current through the junction.

(b) The insulator layer reduces the majority carrier current by reducing their tunneling probability.

(c) The insulator layer contains dipoles which support the photogenerated voltage and thereby reduces dark current.

The tunneling probability of the photogenerated carriers must be 1. The tunneling probability T_a of the photogenerated electrons at the absorber valence band depends on the insulator thickness as follows:

$$T_a = \exp(-\chi_a^{1/2} \delta) \dots\dots\dots\dots\dots\dots\dots\dots (21)$$

where χ_a is the average barrier height of insulator semiconductor interface and δ is the oxide thickness. The total current density in an SIS solar cell is given by

$$J = J_L - J_d - J_{re}^* \quad \text{(oxide layer dependent)} \ldots \quad (22)$$

where J_L, J_d and J_{re}^* are photogenerated current, dark current and recombination current density (dependent on oxide thickness) respectively.

2.5 Solar cell characterization.

2.5.1 Short circuit current (I_{sc}).

This is the maximum current which flows from the front to the back contact without any voltage when the back and front contacts are connected to one another. The total diode current under illumination is given by

$$I = I_1 + I_0 (1 - e^{qv/KT}) \ldots\ldots\ldots\ldots\ldots\ldots \quad (23)$$

where I_0 is the saturation current, I_1 is the light generated current and the second term is the reverse diode current. For uniform absorption, the light current I_1 is given by

$$I_1 = q G_1 (L_n + L_p) A \ldots\ldots\ldots\ldots\ldots\ldots\ldots \quad (24)$$

where G_1 is the generation rate.

32

2.5.2 Open circuit voltage (V_{oc}).

The open circuit voltage can be obtained by setting $I=0$ in equation 23, and thus

$$V_{oc} = (KT/q) \ln (1 + I_1/I_0) \dots\dots\dots\dots\dots \quad (25)$$

In an open circuited cell, no current flows but the voltage generated is maximum.

2.5.3 Fill Factor (FF).

Fill factor is defined as the ratio

$$V_{mp}I_{mp} / V_{oc}I_{sc} \quad \dots\dots\dots\dots\dots\dots\dots\dots\dots \quad (26)$$

This is useful as a measure of the realizable power from the I-V curve. Typical values for a commercial cell lie in the range 0.7 to 0.8.

2.5.4 Efficiency (η)

The solar cell can supply a current if an external load is connected across it. The power delivered to the load is thus

$$P = I V = I_1 V - I_0 V (e^{qV/KT} - 1) \dots\dots\dots \quad (27)$$

The voltage corresponding to the maximum power delivery

33

V_{mp} is obtained by taking $\partial p/\partial V = 0$ in equation (27), hence

$$(1 + qV_{mp}/KT)e^{(qV/KT)} = 1 + I_1/I_o \quad \ldots \ldots \ldots \quad (28)$$

Current at maximum power is denoted I_{mp}. The solar cell efficiency (η) is

$$\eta = (I_{mp}V_{mp} / P_{in}) \times 100 \quad \% \quad \ldots \ldots \ldots \ldots \quad (29)$$

or

$$\eta = \frac{V_{oc} I_{sc} FF \times 100}{P_{in}} \quad \% \quad \ldots \ldots \ldots \ldots \ldots \quad (30)$$

where P_{in} is the input light power. I_{mp} and V_{mp} are the maximum current and voltage respectively achieved in a solar cell.

2.5.5 Series resistance (R_s) and Shunt resistance (R_{sh}).

For an ideal solar cell the series resistance is zero and the shunt resistance is infinity. Commercial cells have series resistance in the range 1 to 5Ω. Series resistance (R_s) is due to the resistivity of the bulk materials, the resistance of the depletion region and the the resistance of the contacts. Shunt resistance (R_{sh}) results from junction defects which determine leakage current across junction (Fig. 12).
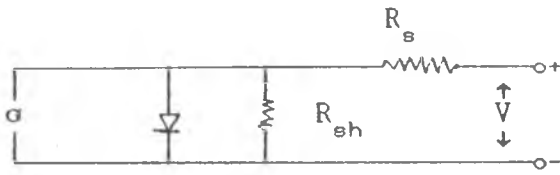
Fig. 12 *Equivalent circuit of a solar cell*

The series resistance of the cell can be obtained by illuminating the cell at two different intensities and plotting their I-V characteristics [35]. This is illustrated in Fig. 13 .
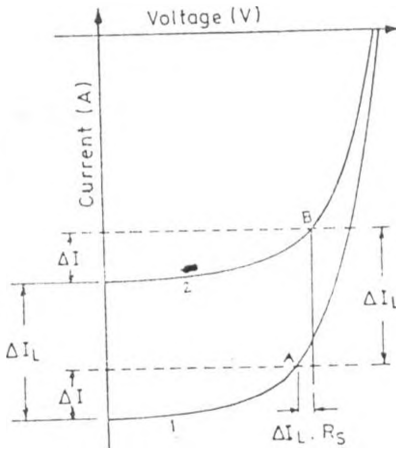
Fig. 13 *Method for determining the series resistance of a cell from I-V curves at two different intensities.*

It is not necessary to know the magnitudes of the intensities. We choose an arbitrary interval ΔI from the I_{sc} point and obtain the point A on curve 1, near the knee of the characteristics. Similarly, taking the same ΔI value, we obtain the point B on curve 2. The points A

and B are displaced relative to each other on the x-axis by an amount $\Delta V = \Delta I_L R_s$, whence the value of R_s can be easily calculated.

The series resistance can also be obtained from the dark I-V characteristics of the cell. The equation for such a case is

$$I = I_0 \left[\exp[(q/mKT)(V - IR_s)] - 1 \right] \quad \dots\dots\dots \quad (31)$$

where I_0 is the saturation current and R_s is the series resistance.

CHAPTER THREE

EXPERIMENTAL TECHNIQUES

3.1 Introduction.

In this chapter experimental techniques employed in deposition of thin tin oxide films, fluorine doping, optical measurements of thin SnO_2 films and fabrication of solar cell are discussed.

Although a variety of methods [23,24,36,37] have been used for SnO_2 deposition, chemical vapour deposition (CVD) and reactive sputtering are the most promising ones [38]. In the present work chemical vapour deposition was used to deposit SnO_2 thin films.

Chemical vapour deposition is the process by which the non-volatile products of a gas phase reaction are allowed to deposit onto a substrate. This process may be further classified by the type of chemical reaction used such as thermal decomposition, reduction, disproportionation and polymerization. The large number of possible chemical reaction allows the formation of films of a wide range of materials on metal or insulating substrates of variable geometry. In contrast to thermal evaporation and sputtering, chemical vapour deposition is possible at atmospheric pressures.

3.2 SnO₂ thin film deposition.

The method used for SnO_2 films is similar to the one used by Vlahovic and Persin [25] but in this study $SnCl_4$ was used as starting material in place of SnI_4. The schematic diagram of the apparatus is shown in Fig. 14.
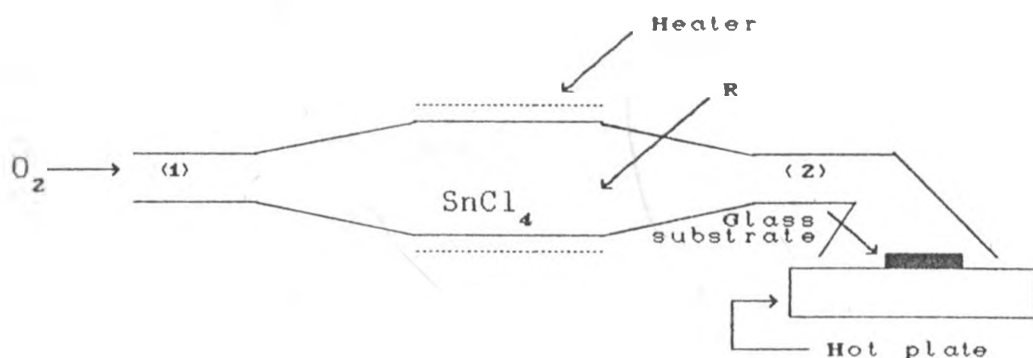
*Fig.14   Schematic diagram for SnO₂ thin film deposition
          by a modified CVD method.*

Carrier gas (Oxygen) passes through pipe 1.   In   the reservoir R, the the starting material $SnCl_4$ is   heated till it sublimes.   The sublimation vapours are carried away through pipe 2   to   the   glass   substrate (2.5x2.5 cm^2) placed on a hot plate.   A   copper-constantan   thermocouple monitored the   substrate   temperature.   When   sublimation vapours of $SnCl_4$ molecules reach   the   heated   substrate, they receive enough energy to   interact   with   oxygen   and the following chemical reaction takes place:

$$SnCl_4 + O_2 \longrightarrow SnO_2 \downarrow + 2Cl_2 \uparrow \ldots\ldots\ldots\ldots \quad (32)$$

The films were removed immediately after deposition.

3.3 Calibration of hot plate temperature with variac dial (voltage).

The hot plate was calibrated in order to record accurate temperatures. The schematic diagram of the set up used for calibration is shown in Fig. 15.
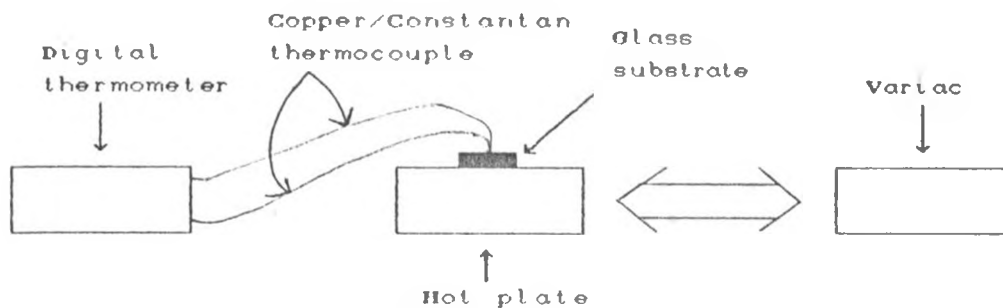
Fig. 15 *Schematic diagram of the set up for hot plate temperature calibration with voltage.*

Thermocouple was made of copper and constantan wires (S.W.G. 30). The fusing of the thermocouple was done by use of a spot welder machine.

Connections were done as per the schematic diagram (Fig.15) and variac dial (voltage) adjusted to 20. The hot plate was left to heat up for $1\frac{1}{2}$ hours (so that the temperature stabilized), temperature was recorded using the digital thermometer. The procedure was repeated for variac dials 40, 60, 80, ... , 240 and the results were tabulated (Table 3). Calibration graph used throughout this study is shown in Fig. 16.

Table 3. Calibration data for hot plate

Variac dial (Voltage)	Temperature ($^{\circ}C$)
0	24.0
20	35.3
40	56.3
60	87.8
80	111.2
100	165.0
120	197.0
140	213.6
160	254.0
180	281.4
200	307.9
220	353.8
240	372.5
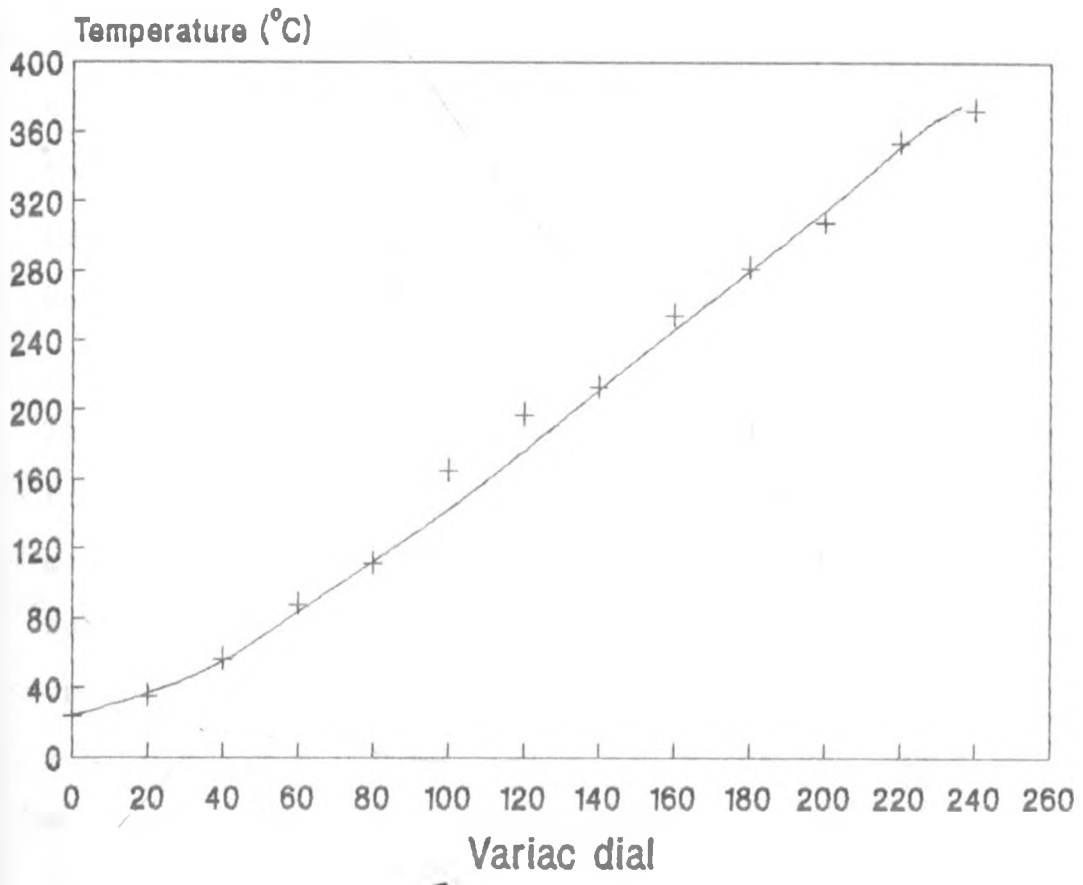
Fig. 16 Calibration graph for hot plate

3.4 Sample preparation for optical measurements.

To obtain optical properties of thin film, cut glass slides size (2.5×2.5 cm^2) were cleaned by detergent, distilled water and finally acetone. The glass slides were then dried in an oven at temperature of 200°C. SnO$_2$ thin film was then deposited on the glass slides by CVD. The films were removed immediately after deposition.

The SP8-150 spectrophotometer was used to determine the transmittance of the film. This was done by putting a blank glass substrate in the reference beam and the coated substrate in the sample beam. The spectral range was set up $0.3 < \lambda < 0.4$ μm for ultra violet region and $0.4 < \lambda < 0.8$ μm for visible region. Back correction was done to set the ordinate display to 100% transmittance. The specimen is then run on the spectrophotometer for transmittance measurements.

Two probe method was used to measure the sheet resistance of the films. Fig. 17 shows the schematic diagram of the set up for sheet resistance measurement.

Intelligent multimeter

SnO$_2$ thin film coated glass substrate

κ Aluminium foil
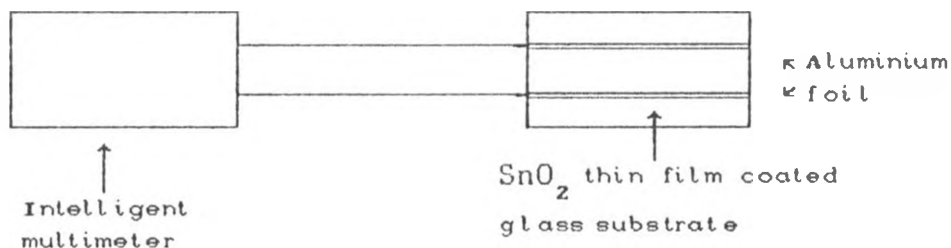
Fig. 17 Schematic diagram of the set up for sheet resistance measurements.

3.4.1 Thickness measurement.

The thickness of the films was found by interference method. This was done by means of fringes observed in the visible region of the transmittance curve of the thin film.

The index of refraction of the substrate (n_2) is about 1.5 and since the film has relatively high index ($n_1=1.9$) [25], then the reflection is the main source of light loss. The thickness (t) of the film can be calculated from equation 33 [39].

$$t = M\lambda_1\lambda_2 / 2 \{ n_1(\lambda_1).\lambda_2 - n_1(\lambda_2)\lambda_1 \} \quad \ldots \ldots \quad (33)$$

where M is the number of oscillations between two extreme values occurring at λ_1 and λ_2, $n_1(\lambda_1)$ and $n_1(\lambda_2)$ are the corresponding refractive indices for the film index (n_1) at wavelengths λ_1 and λ_2.

3.4.2 Bandgap determination.

A ratio recording technique [40] was employed to determine the band gap of the films.

In this technique the transmittance of the thicker film relative to the thinner film is measured. A thin sample was placed in the reference beam and the thicker sample was

placed in the sample beam. The net result is equivalent to measuring the transmission of a hypothetical thin film without reflectance losses of a thickness equal to the difference in thickness of those actually used.

If T_{1-2} is the ratio of transmission and Δt is the thickness difference then

$$T_{1-2} = \exp (-\alpha \Delta t) \dots\dots\dots\dots\dots\dots\dots\dots \quad (34)$$

where α is the absorption coefficient. From equation 31

$$\alpha \Delta t = \ln \frac{1}{T} \dots\dots\dots\dots\dots\dots\dots\dots\dots\dots\dots \quad (35)$$

hence one can accurately calculate $\alpha \Delta t$.

For direct transition, a plot of $(\alpha \Delta t h\nu)^2$ against $h\nu$ where $h\nu$ is the indirect energy, gives a straight line which on extrapolation cuts the energy axis at the band gap. For indirect transition a plot of $(\alpha \Delta t h\nu)^{1/2}$ against $h\nu$ gives a graph which on extrapolation of the straight line part cuts the energy axis at the band gap value [20,37].

It is important to note that the ratio recording technique was applied for transmissions of films in and around the cut-off region.

3.4.3 Preparation of Fluorine doped SnO_2.

Fluorine doping was done by heating the as-grown SnO_2 films together with Ammonium Fluoride (NH_4F) for $2\frac{1}{2}$ minutes at temperatures of $380^{\circ}C$. The set up is shown in Fig. 18.
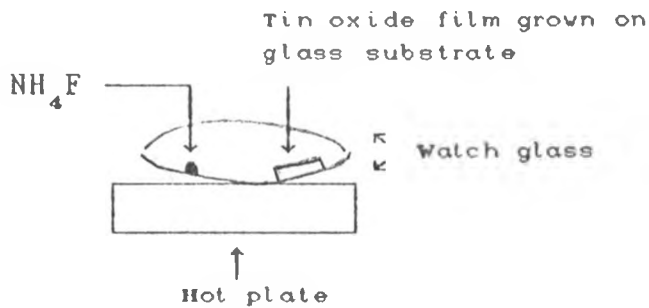
Fig. 18 Set up for SnO_2:F preparation

The degree of doping by Fluorine was controlled by varying the tin (Sn) and Fluorine (F) ratio, [F] / [Sn]. In order to get for example 1% F/Sn doping films prepared with 1 mole of $SnCl_4$ compound were heated together with 0.01 mole of NH_4F.

3.4.4 Cell fabrication.

A 100 Ω-cm p-type (111) boron doped silicon wafer was cleaned in acetone, thoroughly rinsed in deionised water and then dipped into solution containing $\frac{1}{2}$ HF + $\frac{1}{2}$ deionised water (ie. 50% HF solution) to remove the native oxide. After five minutes the wafer was thoroughly rinsed in

distilled water and an oxide layer was grown by placing the wafer in concentrated nitric acid at 60°C for about twenty seconds. The wafer is again cleaned with distilled water.

The substrate (silicon wafer) was then placed on a hot plate at temperature of 365°C and tin oxide layer grown on the polished side of the wafer by chemical vapour deposition. Vacuum coating unit was used to apply aluminium back contact to the unpolished side of the wafer. aluminium grid was made on the front side by placing a grid mask on the top of the polished side of the substrat e (on which a tin oxide layer has been grown) and depositing aluminium by using the vacuum coating unit. The vacuum coating system used was "Hind Hivac" vacuum coating unit model No. 12A4 [41]. This system is capable of giving a vacuum of about 1×10^{-6} Torr.

3.4.5 Cell characterization.

The circuit below (Fig. 19) was used for I-V characteristic measurement of the solar cell. Fig. 20 shows solar cell holder for I-V measurement.
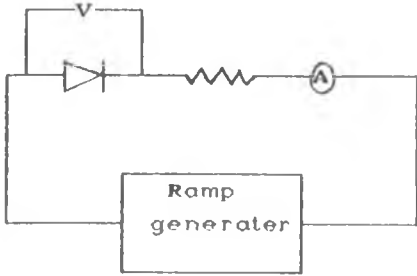
Fig. 19   Circuit for I-V measurement of solar cell.
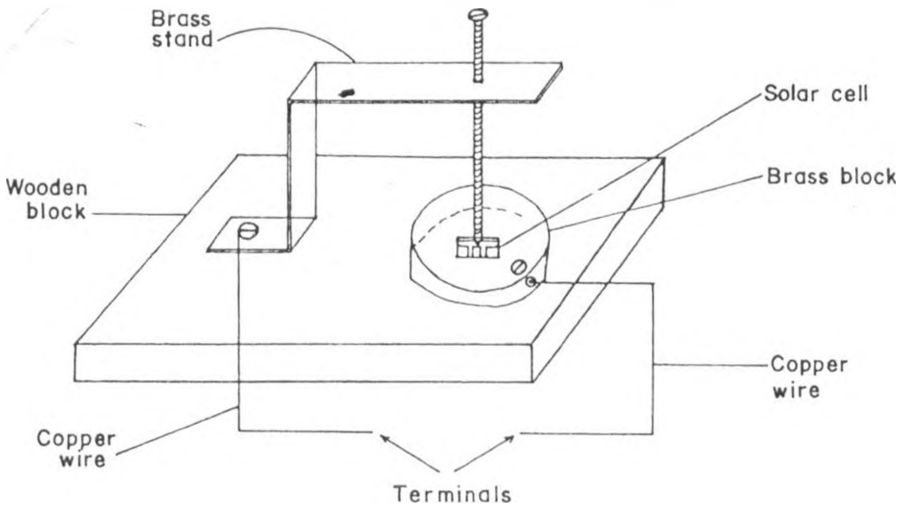
Fig. 20   Solar cell holder.

The light I-V characteristics were obtained by illuminating the solar cell (diode) with a white light source at appropriate distance to give insolation of 80mW/cm^2. A ramp generator was used to vary the voltage.

The dark I-V characteristics were done in a similar fashion as above except that the solar cell (diode) was covered so as not to be exposed to light.

CHAPTER FOUR

RESULTS AND DISCUSSION

4.1 Properties of SnO_2:F films grown by Chemical Vapour Deposition (CVD).

In this section electrical and optical properties of SnO_2:F thin films grown by CVD are discussed. Preliminary results gave the gas flow rate as $1lbf/in^2$ (approx. $7 \times 10^3 NM^{-2}$), mass of Stannic Chloride as 1.5g. and time of coating as 2 minutes for low sheet resistance films.

4.1.1 Electrical properties.

Table 4 shows sheet resistances for SnO_2 films coated at different substrate temperatures. The results are shown graphically in Fig. 21.

Table 4 Values for variac dial, substrate temperature and sheet resistance.

Variac dial	Substrate temperature (°C)	Sheet resistance(Ω/□)
212	336	2900.0
216	344	1742.0
224	358	407.0
228	365	208.4
232	370	314.6
236	375	436.6
240	384	988.2

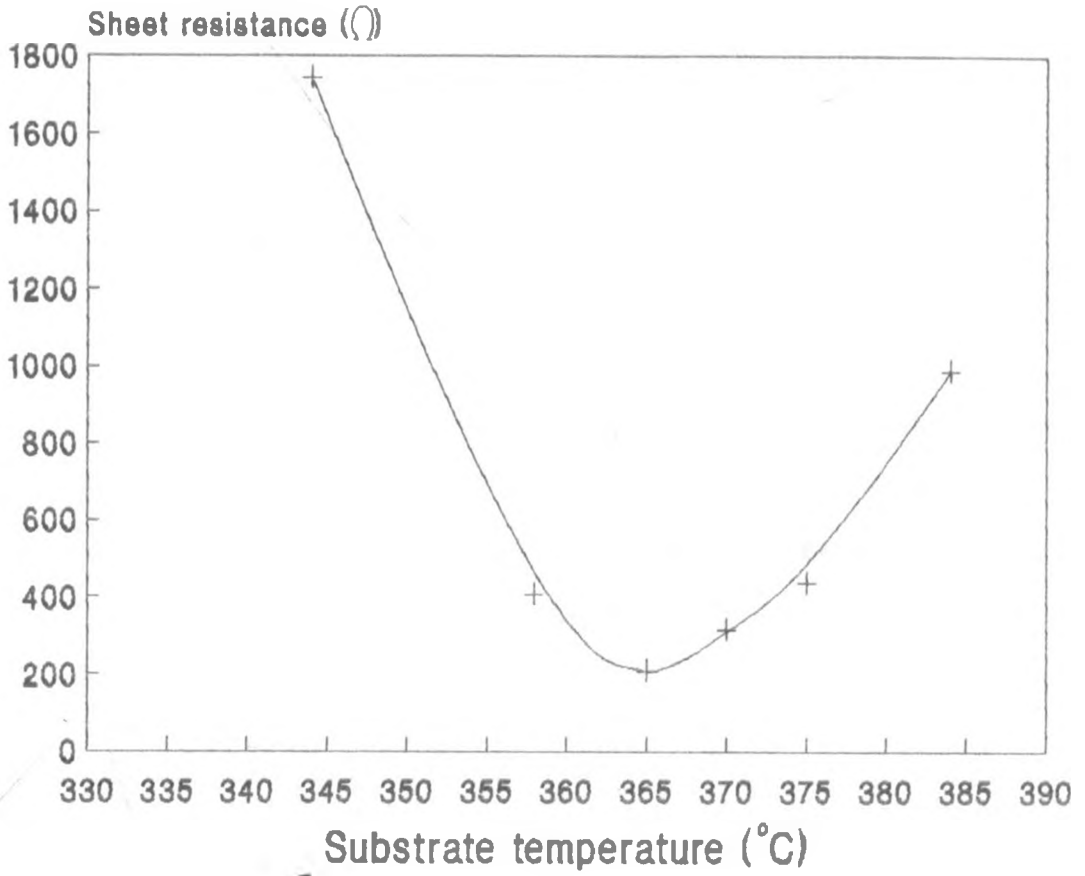Sheet resistance (Ω)

Substrate temperature ($^{\circ}$C)

Fig. 21   *Graph of sheet resistance versus substrate temperature for SnO$_2$* films coated at different temperatures.

Fig. 21 shows a drop in sheet resistance as temperature rises and after a minimum it rises. The optimum substrate temperature for coating SnO_2 films is found to be $365^{\circ}C$. Sheet resistances are high for both substrate temperatures lower and higher than $365^{\circ}C$. This might be due to incomplete reaction at lower substrate temperatures and cracked films at higher substrate temperatures.

The transmission spectra for SnO_2 thin films with sheet resistances of 208.4 $\Omega/\square$, 407.0 $\Omega/\square$, and 2900.0 $\Omega/\square$ grown at substrate temperatures 365, 358 and $336^{\circ}C$ respectively are shown in Fig. 22. It is seen that the absorption edge of lower resistivity film is shifted towards lower energy side. Similar results have been reported for Cadmium Stannate films [7]. These results are contrary to those reported by Spence on vacuum evaporated films [23]. He found the absorption edge for low resistivity films to be about 0.1 eV higher than that for high resistivity films. Our results can be explained on the basis of degeneracy in SnO_2 films which effectively shifts the absorption edge towards the lower energy side [24].

SnO_2 thin films grown at optimum conditions gave sheet resistances ranging from about 70-250 $\Omega/\square$. Transmission spectra for some SnO_2 films grown at optimum conditions with different sheet resistances is shown in Fig. 23. The absorption edge shifted to the lower energy side for low
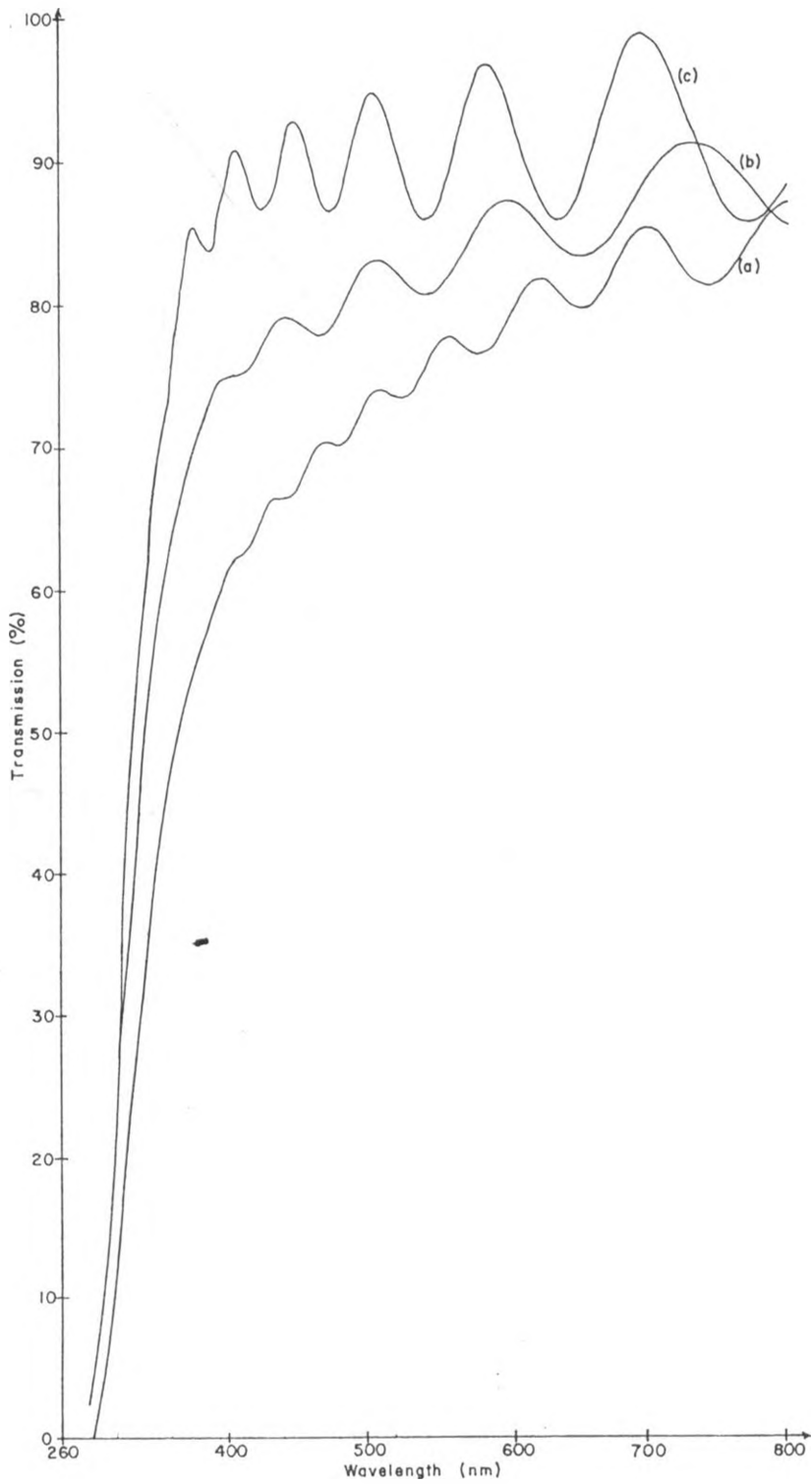
Fig.22 Trasmission spectra for SnO_2 thin films with sheet resistances (a) 208.4 $\Omega/\square$ (b) 407.0 $\Omega/\square$ (c) 2900.0Ω /$\square$
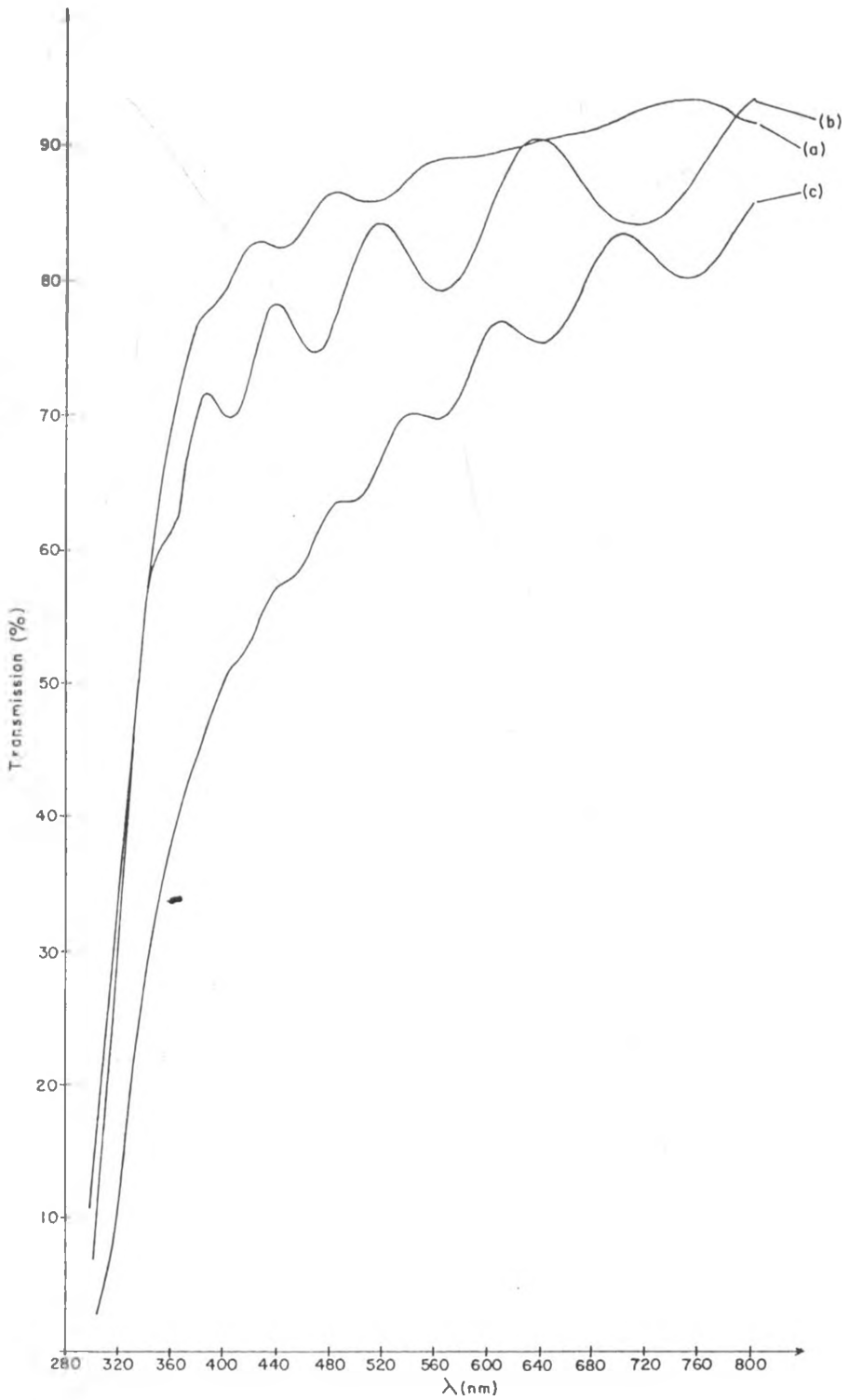
Fig. 23 Transmission spectra for SnO_2 films with different sheet resistances grown at optimum conditions. (a) 210 $\Omega/\square$ (b) 154 $\Omega/\square$ (c) 105 $\Omega/\square$

resistivity films as above.

In – Situ doping of Fluorine by sublimating $SnCl_4$ and NH_4F together was not successful due to high reactivity of Fluorine. Therefore $SnO_2:F$ films were prepared by heating the as-grown films together with NH_4F in a closed atmosphere for two and a half minutes. Table 5 shows the the results obtained.

Table 5   Values of sheet resistance (R_{st}) of SnO_2 films before and after doping.

R_{st} before doping $(\Omega/\square)$	Percentage doping	R_{st} after doping $(\Omega/\square)$
91.7	1	184.7
104.3	2	150.4
130.0	4	145.9
105.1	5	92.3
90.3	6	50.1
109.6	8	74.0
99.2	10	71.5
115.4	20	97.5
121.6	30	124.7
120.7	40	157.2
100.3	50	120.3

From table 5 it can be seen that sheet resistances after doping increases for percentage doping less than 5%, decreases for percentage doping 5-20 %, and increases for percentage doping more than 20%. The increase in sheet

resistance for low percentage doping is due to low concentration of Fluorine and hence it is as if SnO_2 film is being annealed in air at high temperature, while for high percentage doping is due to spoiled film due to high reactivity of Fluorine which spoils the film. The best percentage doping is 6%.

Fig. 24 shows the transmission spectra for a film before and after doping. The amount of NH_4F used was to give 6% F/Sn doping. The sheet resistance decreased from about 90 ohm per square to about 50 ohm per square and the transmission increased by about 5%. This means that doping produces higher transparency and conductivity. The shift in absorption edge towards the higher energy side on doping can be attributed to Moss-Burstein effect which occur owing to filling up of low lying energy levels by the conduction electrons. Similar results have been reported for sprayed antimony doped SnO_2 films [22].

4.1.2 Optical properties.

Direct and indirect bandgap of tin oxide film was found by considering two tin oxide films of different thicknesses. The films were deposited at optimum temperature and pressure but at different times of coating.

Transmittance curves for tin oxide films coated for 2 and 6 minutes are shown in Fig. 25. The thicknesses were found to be 0.136 and 0.205μm for thin films coated for 2 and 6
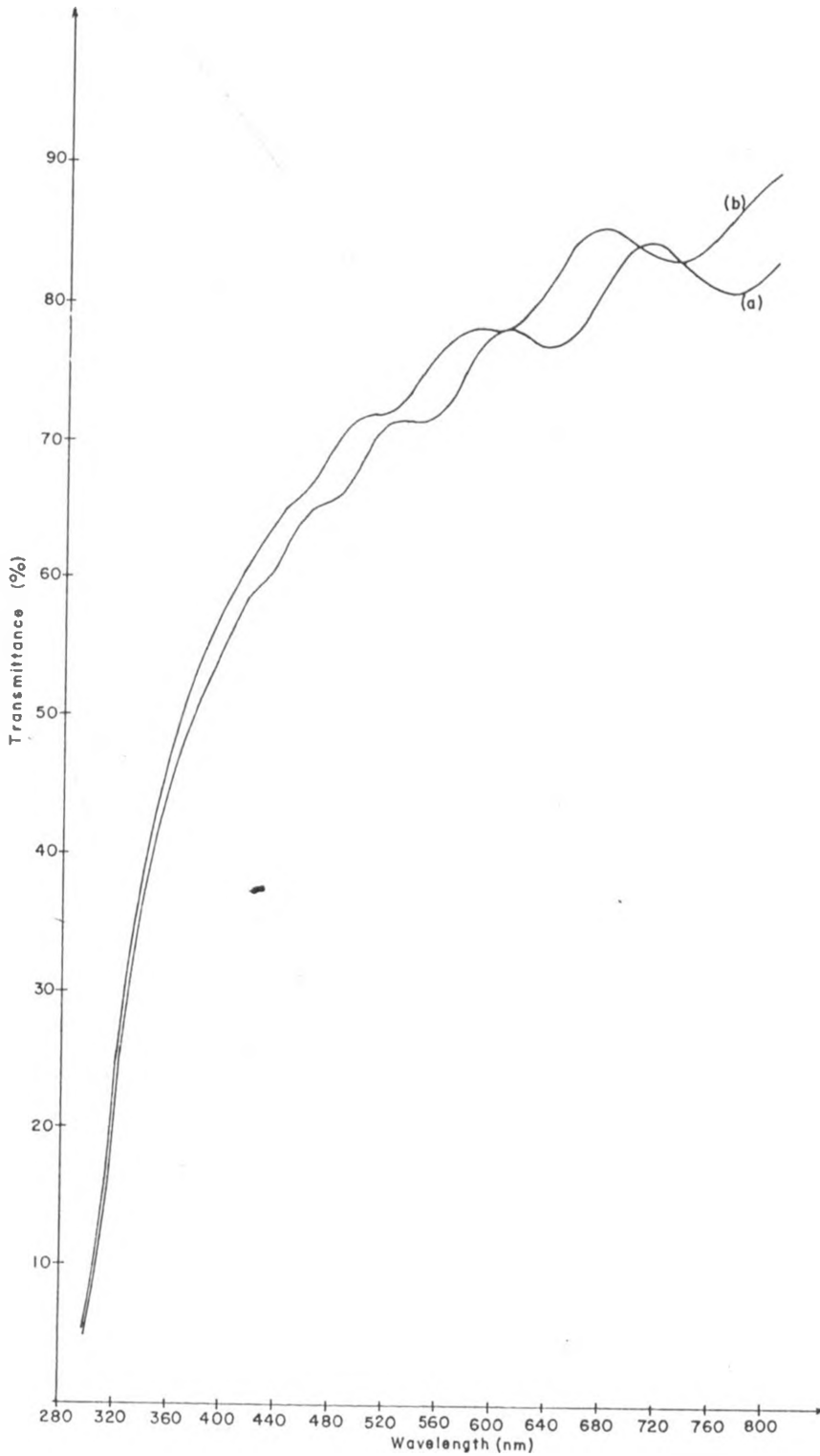
Fig. 24   Transmission spectrum for undoped and doped tin oxide films. (a) Before doping (b) After doping
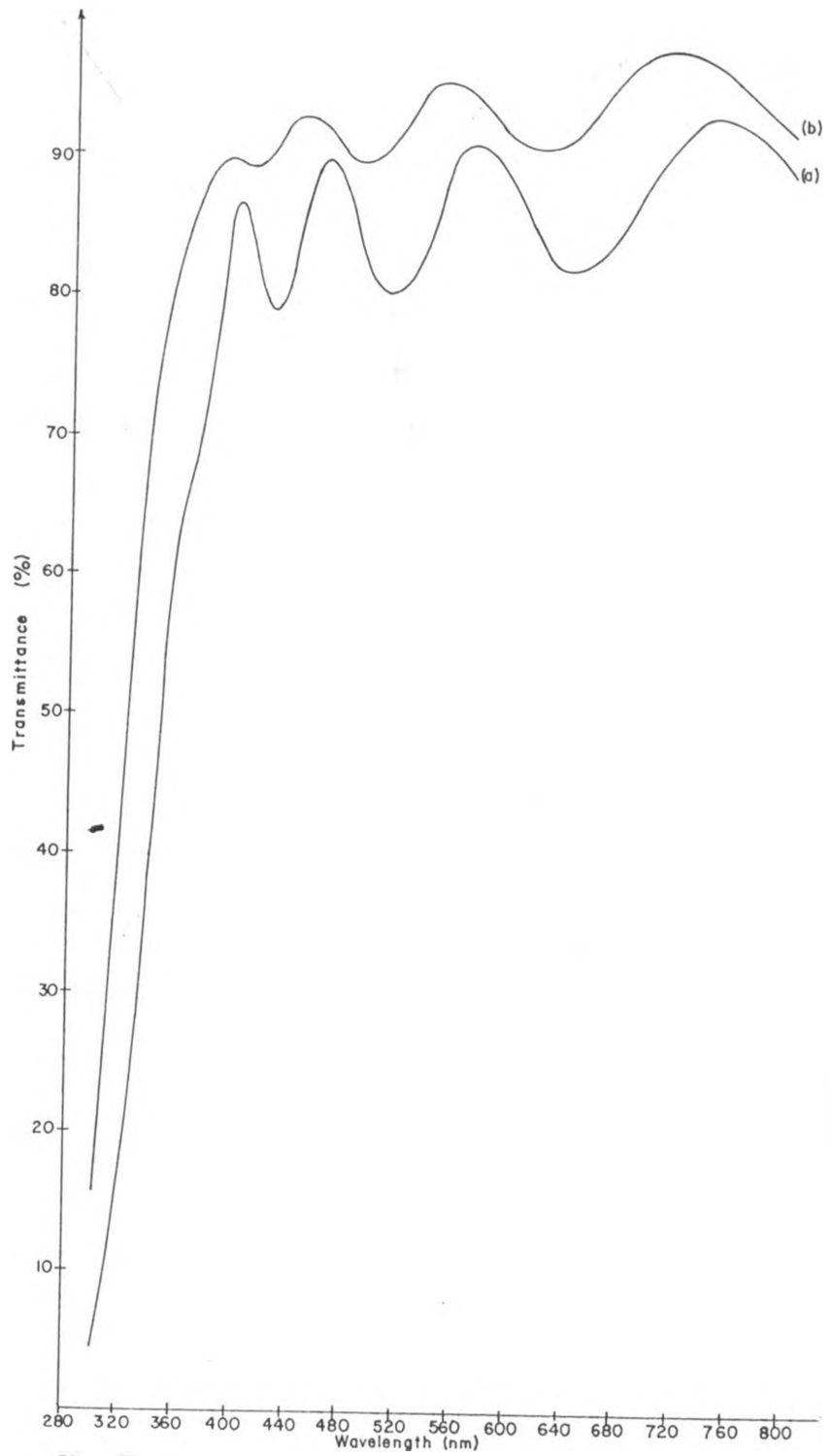
Fig. 25   Transmission spectra for tin oxide films with
different thicknesses. (a) 0.205 μm (b) 0.136 μm

minutes respectively (See Appendix 1). The sheet
resistances were 230Ω/□ and 3.6kΩ/□ for films deposited for
2 and 6 minutes respectively. It is seen that percentage
transmittance for the thinner film is higher than that for
thicker films.

Values in Table 6 were obtained from Fig. 25a from
where a plot of variation of absorption coefficient α
with photon energy was drawn (Fig. 26). The absorption
edge was around 3.5eV. This is close to the value
reported for single crystals [23].

Table 6 Values for variation of absorption coefficient (α) with photon energy.

Wavelength (μm)	Photon energy(hν) (eV)	Transmittance	$\alpha t = \ln \frac{1}{T}$	Absorption coefficient(α) ($10^4 cm^{-1}$)
0.304	4.08	0.045	3.101	15.13
0.312	3.97	0.100	2.303	11.23
0.320	3.88	0.170	1.772	8.64
0.336	3.69	0.340	1.079	5.26
0.344	3.60	0.440	0.821	4.00
0.352	3.52	0.550	0.598	2.92
0.360	3.44	0.640	0.446	2.18
0.368	3.37	0.670	0.400	1.95
0.376	3.30	0.700	0.357	1.74
0.384	3.23	0.760	0.274	1.34
0.400	3.10	0.865	0.145	0.71
0.416	2.98	0.810	0.210	1.02

Ratio recording technique done near the absorption edge yielded Fig. 27 which is a percentage transmittance curve of a thicker tin oxide film relative to a thinner film. From this figure Table 7 which shows different parameters from where plots of $(\alpha\Delta th\nu)^2$ versus $h\nu$ (Fig. 28) and $(\alpha\Delta th\nu)^{1/2}$ versus $h\nu$ (Fig. 29) were drawn.
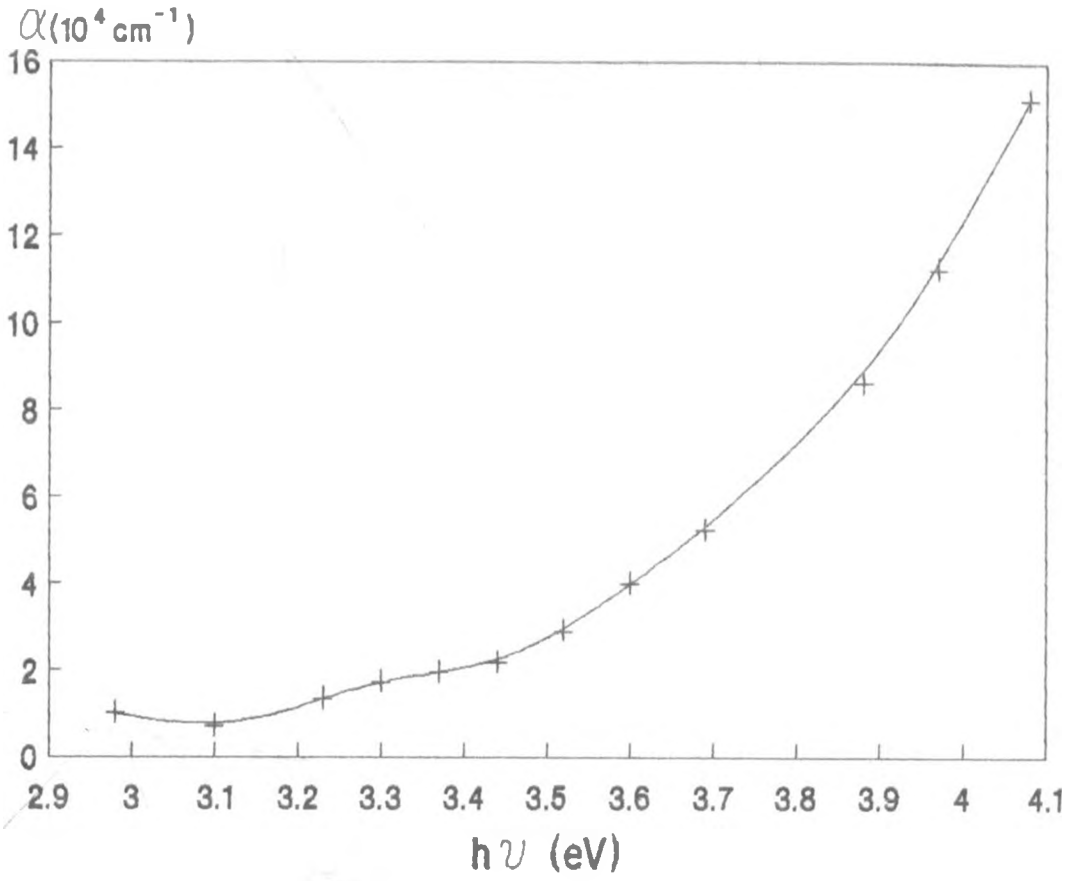
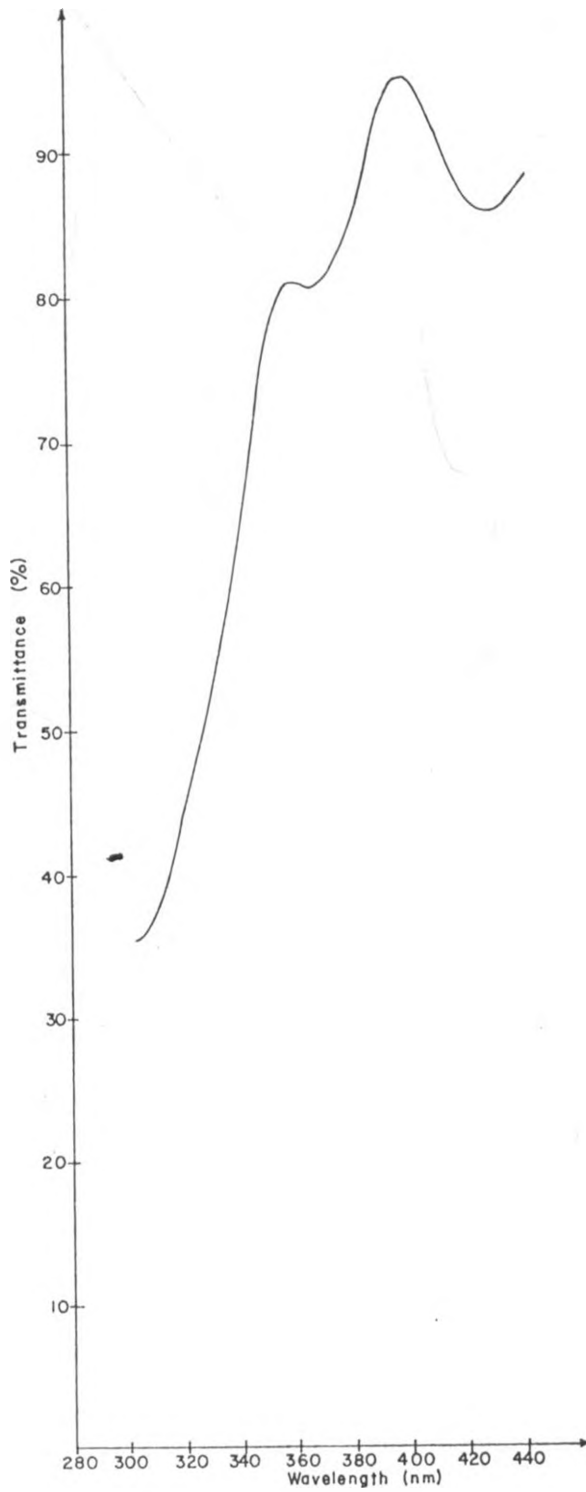Fig. 26   Variation of absorption coefficient α   with
          photon energy.

Fig. 27   Relative percentage transmission spectra for films
with thicknesses   0.136   and 0.205 μm.

Direct and indirect bandgap values of tin oxide films were obtained by extrapolation of the plots. The direct and indirect bandgap values of SnO_2 thin film were found to be 3.55 and 3.19 eV respectively. For single crystals direct bandgap values are reported as 3.57-3.7 eV and indirect bandgap of 3.4 eV [42]. Spence [23] has reported a direct bandgap of 4.45 eV and indirect bandgap of 3.05eV for evaporated films. Abbas and Mohammed [21] determined a direct bandgap of 4.13 eV and an indirect bandgap of 2.69 eV with assisting phonon of 0.085 eV for sprayed SnO_2 films.

Table 7   Values for wavelength, transmittance, $(\alpha\Delta t h\nu)^2$ and $(\alpha\Delta t h\nu)^{1/2}$.

Wavelength (μm)	Photon energy(hν) (eV)	Transmittance	$\alpha\Delta t$	$(\alpha\Delta t h\nu)^2$ (eV)^2	$(\alpha\Delta t h\nu)^{1/2}$ (eV)$^{1/2}$
0.320	3.88	0.45	0.85	9.63	1.76
0.324	3.83	0.47	0.76	8.47	1.71
0.328	3.78	0.50	0.69	6.80	1.61
0.332	3.73	0.53	0.63	5.52	1.53
0.340	3.65	0.62	0.48	3.07	1.32
0.348	3.56	0.735	0.31	1.22	1.05
0.356	3.48	0.81	0.21	0.53	0.85
0.360	3.44	0.81	0.21	0.52	0.85
0.370	3.35	0.815	0.20	0.45	0.82
0.380	3.26	0.86	0.15	0.24	0.70
0.390	3.18	0.92	0.08	0.06	0.50
0.400	3.10	0.95	0.05	0.02	0.39
0.420	2.95	0.87	0.14	0.17	0.64
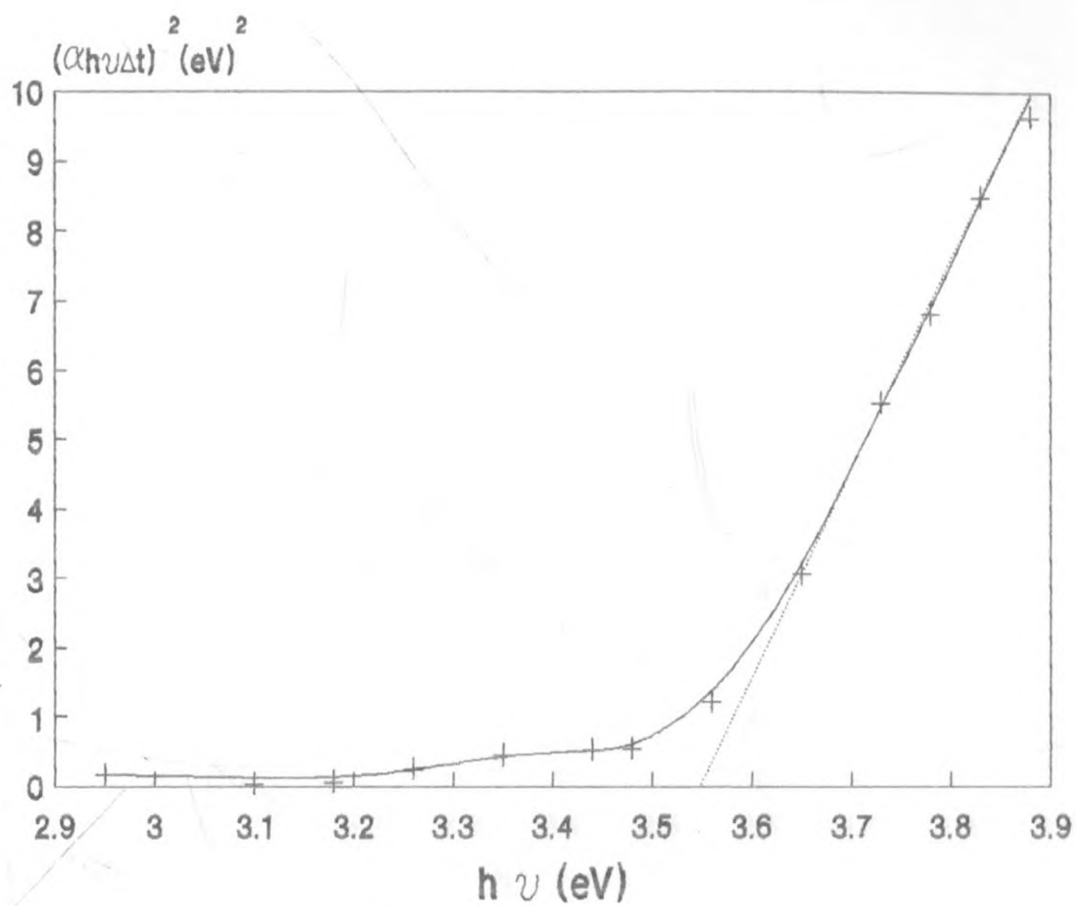
Fig. 28 Plot of $(\alpha \Delta t h\nu)^2$ versus $h\nu$.
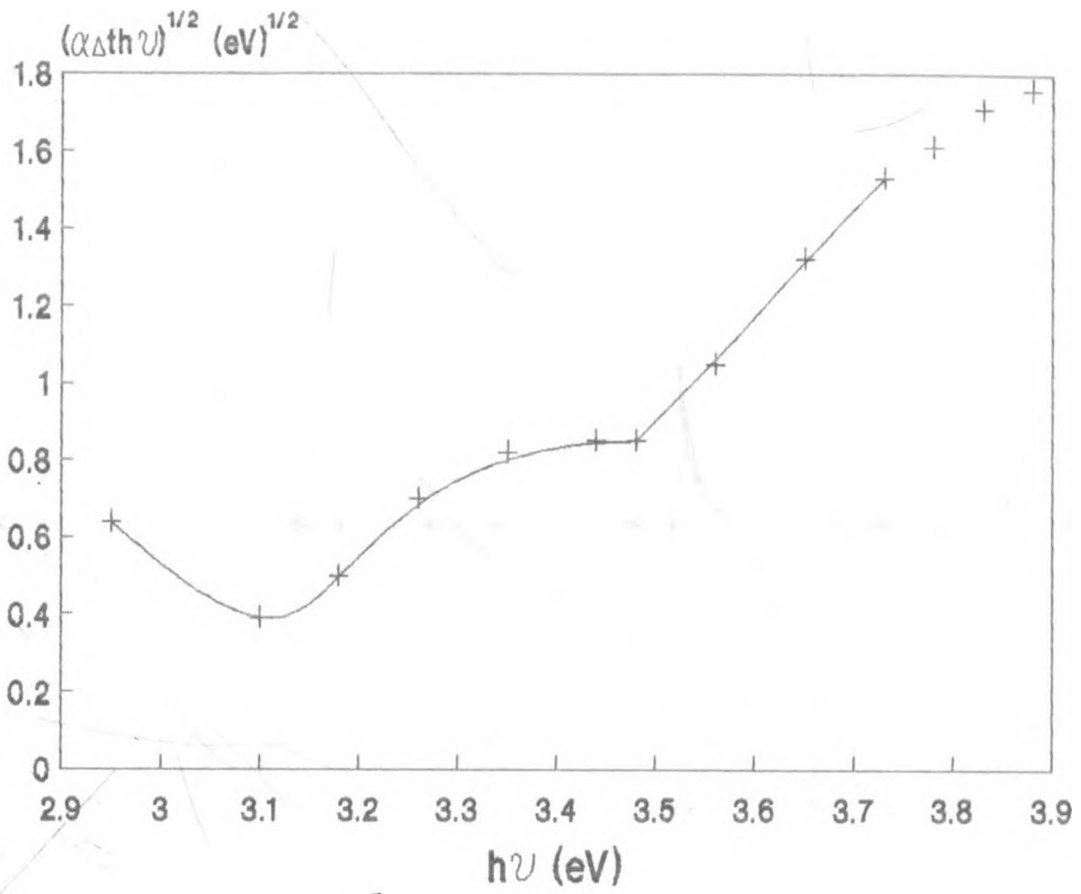
Fig. 29   Plot of $(\alpha \Delta t h\nu)^{1/2}$ versus $h\nu$

4.2   Characterization of $SnO_2:F/SiO_2/p-Si$ Solar cell.

4.2.1   I-V characteristics.

Dark   I-V   values are shown in   Table   8   while light   I-V
values under   80mW/cm   insolation are shown in Table   9.

Table 8   Dark   I-V characteristics values.

Voltage (V)	Current density ($\mu A/cm^2$)
0.00	0.0
0.10	22.2
0.13	33.3
0.16	44.4
0.18	55.6
0.20	66.7
0.26	111.1
0.30	144.4

Table 9 Light I-V characteristics values under 80mW/cm insolation.

Voltage (V)	Current density ($\mu A/cm^2$)
0.07	411.1
0.10	333.3
0.11	311.3
0.12	288.9
0.13	266.7
0.14	244.4
0.20	100.0
0.21	66.7
0.24	22.2
0.25	0.0

Fig. 30 shows dark I-V characteristics and light I-V characteristics under 80mW/cm^2 insolation.

The cell parameters obtained are:

Open circuit voltage, V_{oc} = 0.25 V

Short circuit current density, J_{sc} = 556$\mu A/cm^2$

Fill factor = 0.23

Cell efficiency = 0.04%

The efficiency of SnO_2:F/ S iO_2/p-Si solar cell is low. SIS solar cells operate on principle of minority carrier tunneling through an oxide layer. The silicon surface is accumulated by virtue of SnO_2 work function. As a result the barrier height is increased hence few minority
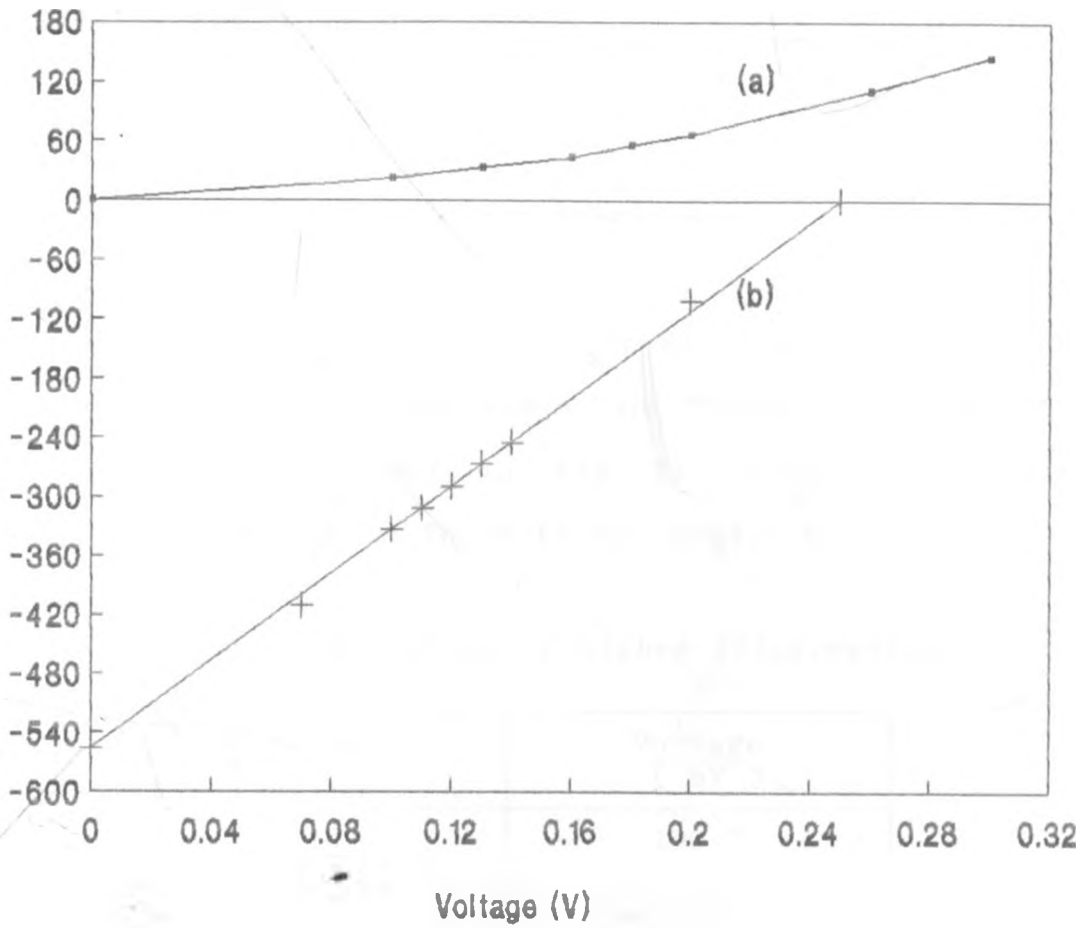
Fig. 30 (a) *Dark I-V characteristics of* $SnO_2:F/SiO_2/p-Si$
        solar cell.

        (b) *I-V characteristics of* $SnO_2:F/SiO_2/p-Si$ *solar*
        cell under 80mW/cm^2 insolation.

carriers (electrons) will tunnel through the Si-SiO$_2$ junction to combine with the photogenerated holes. This will greatly limit the photocurrent being drained from the cell.

4.2.2 Determination of series resistance.

Light I-V values for SnO$_2$:F/SiO$_2$/p-Si solar cell at different illuminations are shown in Tables 10 and 11. The power curves are shown in Fig. 31. From the figure the series resistance is found to be 3294.1 Ω.

Table 10. Light I-V values (higher illumination)

Current (μA)	Voltage (mV)
18	190.7
22	175.7
26	162.5
30	149.0
34	136.3
38	122.7
42	110.2
46	97.5
50	84.9
54	72.3
58	61.7
60	58.8

Table 11 Light I-V values (lower illumination)

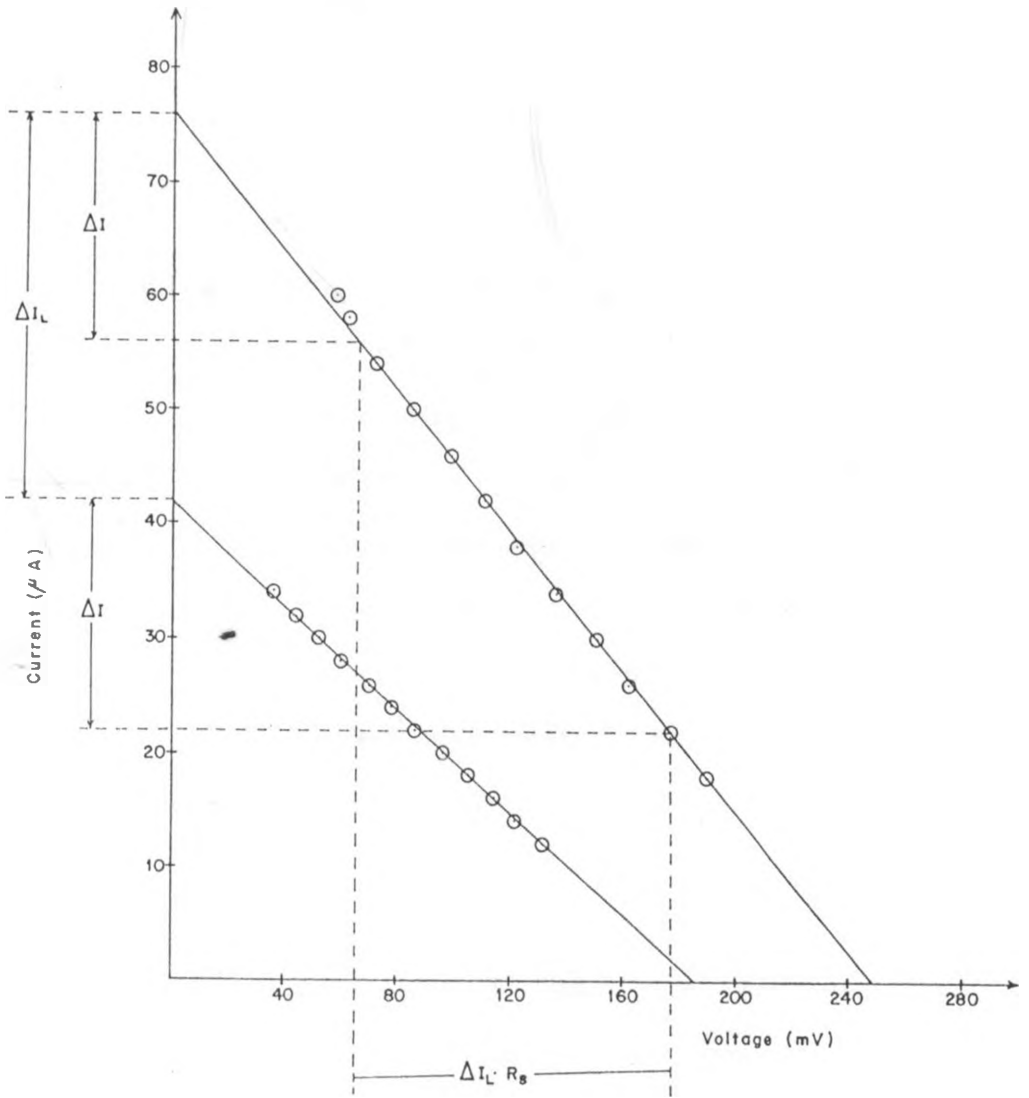| Current (µA)	Voltage (mV)
12	131.4
14	122.9
16	114.8
18	105.0
20	95.8
22	86.8
24	78.1
26	70.2
28	60.4
30	52.5
32	43.7
34	35.1

Fig. 31   *I-V power curve under two different illuminations.*

CHAPTER FIVE

CONCLUSION AND SUGGESTIONS FOR FURTHER WORK

5.1   Conclusion.

Chemical vapour deposition has been used to fabricate SnO_2 and SnO_2:F thin films. The optimum substrate temperature for depositing SnO_2 films was found to be 365°C. The direct and indirect bandgap values of SnO_2 films were found to be 3.55 and 3.19 eV respectively which are comparable to the values obtained by otherworkers. The films were transparent in the visible and exhibited interference colours. The reflection was less than 20% throughout the visible range. The uniformity of the films is apparent from the presence of interference fringes in the transmission spectrum. Films grown with $SnCl_4$ as starting material seem to have better optical properties than those grown with SnI_4. The transmission spectrum of the latter films did not indicate homogeneity of the cross section [25].

SnO_2:F gave a sheet resistance of 50Ω per square. The possible cause for such a resistance is the resistance between the film and the contacts. Sheet resistance less than 20Ω per square has been reported by other workers.

The transmittance of SnO_2:F films was about 85%. High transmittance and high conductivity are ideal for their

application in transparent semiconducting photovoltaic devices.

The efficiency of SnO_2:F/SiO_2/p-Si solar cell was found to be 0.04%. This low efficiency might be due to the incompatibility of two materials, high series resistance and insulater thickness. This may be enhanced by use of n-type silicon of low resistivity and improving SnO_2:F deposition technique. Poor contacts and junction defects also contributed to the low efficiency obtained. This efficiency is better than that of a similar cell fabricated by Kalaiya [13]. It is however much lower to the 12% achieved for a SnO_2:F/SiO_2/n-Si solar cell reported by Singh et al [8].

This technique of fabricating SnO_2 films and hence SIS solar cell is better than spray pyrolysis method both in terms of costs and simplicity. The results (i.e. sheet resistance of SnO_2 films, efficiency of SnO_2:F/SiO_2/p-Si solar cell) obtained in Physics laboratory, Nairobi University are also better using this technique than those obtained by spray pyrolysis.

5.2 Suggestion for future work.

The sheet resistance for SnO_2 and SnO_2:F thin films obtained was high. This needs to be reduced to less than 10Ω per square. The chemical vapour deposition apparatus used can be modified to get such a result. A lot of work

should also be done on determining the optimum conditions for SnO_2 thin films deposition. Attention should be paid to substrate temperature, gas flow rate and time of coating.

n-type Silicon wafer with resistance less than 10Ω-cm ought to be used to make more efficient cells. In this work $100\ \Omega$-cm p-type Silicon wafer was used. The cleaning process applied to the Silicon wafers needs some improvement to reduce contamination. Contamination can result from dirty tools and improper handling of the wafers. Some means of measuring oxide thickness is essential as thickness needs to be optimized. This can be done by using ellipsometry. Aluminium was used to form ohmic contacts. To improve the performance of the cells, the resistance at the metal-semiconductor boundary should be eliminated by reducing the grain-boundary effects.

It is believed that better results can be obtained with improved fabricating procedures.

Thickness calculation.

The thickness of the film was calculated by using equation 30. In this region (visible region) the thickness of film (n_1) is nearly constant hence $n_1(\lambda_1) = n_2(\lambda_2)$. Below are values for λ s, M and thickness for thinner and thicker films.

Thinner film (coated for 2 minutes).

	Peaks	Troughs	Average thickness (μm)
λ_1 (μm)	0.448	0.408	
λ_2 (μm)	0.720	0.624	
M	2	2	
Thickness(μm)	0.167	0.104	0.136

Thicker film (coated for 6 minutes).

	Peaks	Troughs	Average thickness (μm)
λ_1 (μm)	0.400	0.428	
λ_2 (μm)	0.748	0.644	
M	3	2	
Thickness(μm)	0.297	0.113	0.205

LIST OF REFERENCES

1. Newsweek magazine, 24, September 18 (1989).

2. Newsweek magazine, 8, May 12 (1986).

3. Cheremisinoff P. N.
    Principles and applications of solar energy.
    (Ann. Arbor Science) (1978).

4. Singh S. P.
    Ph.D Thesis I. I. T. Delhi (1984) (Unpublished).

5. Proceedings of the first contractors meeting held in
    April 1986.
    Photovoltaic power generation - Vol. 1.

6. Garbuny C.
    Optical Physics.
    Academic press New York and London (1965).

7. Agnihotri and Gupta B. K.
    Solar selective surfaces.
    Wiley New York (1984).

8. Singh S. P., Saxena , Tiwari L. M. and Agnihotri O. P.
    SnO_2:F/n-Si and In_2O_3:Sn/n-Si SIS solar cells.
    Thin solid films, 127, 77-84 (1985).

9. Feng T., Ghosh A. K., and Fishman C.
    Efficient electron beam deposited ITO/n-Si solar cells.
    J. Appl. Phys. 50(7),4972, (1979).

10. Born M. and Wolf E.
    Principles of optics.
    Pergamon Press, Fifth edition (1975).

11. Kaye G. W. C. and Laby T. H.
    Tables of physical and chemical constants.
    Longman Group Limited, 49 (1971).

12. Jain V. K. and Kulshresta A. P.
    Solar Energy mater. 4, 151, (1981)

13. Kalaiya N. V.
    Fabrication of a Semiconductor Insulater Semiconductor
    Photovoltaic converter.
    MSc. Thesis (1990).
    University of Nairobi. (Unpublished).

14. Chapin D. M., Fuller C. S. and Pearson G. L.
    A new Silicon p-n junction photocell for converting
    solar radiation into electrical power.
    J. Appl. Phys, 676, (1954).

15. Seraphin B. O.
    Notes on series of lectures given at the " Second
    College on thin film technology" Dar es Salaam,
    Tanzania (3-15 August 1992).

16. Seraphin B. O.
    Review presented at the workshop on Materials, session
    on solar cells, Hanoi, Vietnam, (15-19 October 1990).

17. Singh S. P., Raza A., Sharma A. K., Agnihotri O. P.
    and Tiwari L. M.
    Characterization of Fluorine doped In_2O_3 films
    sythesized by spray pyrolysis.
    Thin solid films, 105, 131. (1981).

18. Schewchen J., Dubow J., Myszkowski A. and Singh R.
    The operation of the Semiconductor Insulator
    Semiconductor solar cell.
    J. Appl. Phys., 49(2), 855.

19. Chang N. S. and Sites J. R.
    Electronic characterization of indium tin oxide/Silicon
    Photodiodes.
    J. Appl. Phys. 49(9), 4833, (1978).

20. Summi R., Marley J. A. and Boncelli N. F.
    The ultraviolet absorption edge of stannic oxide.
    J. Phys. Chem. Solids 25, 1465, (1964).

21. Abass A. K. and Mohammed
    Optical properties of Fluorine doped SnO_2 films.
    J. Appl. Phys. 59(5), 1641, (1986).

22. Shanti E., Dutta V., Benerjee and Chopra K. L.
    Electrical and optical properties of undoped and
    antimony-doped tin oxide films.
    J. Appl. Phys. 51(12), (1980).

23. Spence W.
    The UV absorption edge of tin oxide thin films.
    J. Appl. Phys. 38(9), 3767, (1967).

24. Sundram K.B. and Bhagwat G. K.
    Optical absorption studies on tin oxide films.
    J. Phys. D (Appl. Phys.) 14, 921, (1981).

25. Vlahovic B. and Persin M.
    A simple and new modified CVD technique for
    fabrication of SnO_2 films.
    J. Phys. D (Appl. Phys.) 23, 1324, (1990).

26. Manyonge W. M.
    Technological development of ceramic Cds/Cu_2S solar
    cell.
    MSc. Thesis (1981).
    University of Nairobi. (Unpublished).

27. Ogola B. O.
    Fabrication and charactrization of silicon solar cells.
    MSc. Thesis (1985).
    University of Nairobi. (Unpublished).

28. Cotton F. A. and Wilkinson G.
    Advanced Inorganic Chemistry.
    New York Interscience pub. (1966).

29. Sidgwick N. V
    Chemical elements and their compounds. p.600
    Oxford, Clarendon Press, (1950).

30. Kittel C.
    Introduction to solid state Physics.
    Wiley Eastern Limited 5th Edition (1976).

31. Sze S. M.
    Physics of Semiconductor devices.
    John Wiley & Sons, 2nd Edition (1976).

32. Thomas R. E.
    Solar energy conversion. p. 785-803.
    Pergamon Press, Edited by Dixon A . E. and Leslie I . D.
    (1978).

33. Shewchun J.
    Solar energy conversion. p. 843-884.
    Pergamon Press, Edited by Dixon A . E and Leslie I. D.
    (1978).

34. Shewchun J., Singh R., Burk D., Spitzer M., Loferski J.
    and Dubow J.
    13 Photovoltaic Specialist Conf.(IEEE, New York, 1978)

35. Chopra K. L. and Das S. R.
    Thin film solar cells.
    Plenum Press, New York, (1983).

36. Mohammad M.T. and Abass A. K.
    Optical properties of chemically deposited conducting
    glass for SIS solar cells.
    Phys. stat. sol. (9), 83, 681 (1984).

37. Casey V. and Stephenson M. I.
    A study of undoped and molybdenum doped polycrystaline
    tin oxide thin films produced by a simple reactive
    evaporation technique.
    J. Phys. D; Appl. Phys. 23, (1990).

38. Manifacier J. C.
    Thin metallic oxides as transparent conductors.
    Thin solid films, 90, 297-308, (1982).

39. Jiang Hong Ming, Gao Jin Hua, Li Zhen.
    An experimental study for transparent heat reflecting
    glass coating.
    1st world renewable energy congress,
    vol. 3, p. 1393- 1397, (1990).

40. Manifacier J. C., Carriot J., and Filtard J. P.
    J. Phys. E, 9, 1002, (1966).

41. Hind high vacuum Co(P) LTD, Bangalore, India.
    working instructions of "Hindhivac" vacuum coating
    unit model 12A4.

42. Reddaway and Wright D. A.
    Optical properties of tin oxide crystals.
    Br. J. Appl. Phys. 16, 195, (1965).